CANADIAN THESES ON MICROFICHE

THÈSES CANADIENNES SUR MICROFICHE

National Library of Canada
Collections Development Branch

Canadian Theses on
Microfiche Service

Ottawa, Canada
K1A 0N4

Bibliothèque nationale du Canada
Direction du développement des collections

Service des thèses canadiennes
sur microfiche

NOTICE

The quality of this microfiche is heavily dependent upon the quality of the original thesis submitted for microfilming. Every effort has been made to ensure the highest quality of reproduction possible.

If pages are missing, contact the university which granted the degree.

Some pages may have indistinct print especially if the original pages were typed with a poor typewriter ribbon or if the university sent us an inferior photocopy.

Previously copyrighted materials (journal articles, published tests, etc.) are not filmed.

Reproduction in full or in part of this film is governed by the Canadian Copyright Act, R.S.C. 1970, c. C-30. Please read the authorization forms which accompany this thesis.

AVIS

La qualité de cette microfiche dépend grandement de la qualité de la thèse soumise au microfilmage. Nous avons tout fait pour assurer une qualité supérieure de reproduction.

S'il manque des pages, veuillez communiquer avec l'université qui a conféré le grade.

La qualité d'impression de certaines pages peut laisser à désirer, surtout si les pages originales ont été dactylographiées à l'aide d'un ruban usé ou si l'université nous a fait parvenir une photocopie de qualité inférieure.

Les documents qui font déjà l'objet d'un droit d'auteur (articles de revue, examens publiés, etc.) ne sont pas microfilmés.

La reproduction, même partielle, de ce microfilm est soumise à la Loi canadienne sur le droit d'auteur, SRC 1970, c. C-30. Veuillez prendre connaissance des formules d'autorisation qui accompagnent cette thèse.

THIS DISSERTATION
HAS BEEN MICROFILMED
EXACTLY AS RECEIVED

LA THÈSE A ÉTÉ
MICROFILMÉE TELLE QUE
NOUS L'AVONS REÇUE

Canada

NL 339 (r. 86/08)

National Library of Canada | Bibliothèque nationale du Canada

Ottawa, Canada
K1A 0N4

151

TC –

ISBN 0-315-01345-0

CANADIAN THESES ON MICROFICHE SERVICE – SERVICE DES THÈSES CANADIENNES SUR MICROFICHE

PERMISION TO MICROFILM – AUTORISATION DE MICROFILMER

• Please print or type – Écrire en lettres moulées ou dactylographier

AUTHOR – AUTEUR

Full Name of Author – Nom complet de l'auteur

WILLIAM JOHN RUTLEDGE

Date of Birth – Date de naissance	Canadian Citizen – Citoyen canadien
27 JUNE, 1985	☒ Yes / Oui ☐ No / Non
Country of Birth – Lieu de naissance	**Permanent Address – Résidence fixe**
CANADA	BOX 25, SITE 18, RR6 EDMONTON, ALBERTA T5B 4K3

THESIS – THÈSE

Title of Thesis – Titre de la thèse

AN AIR DISPLACEMENT TECHNIQUE FOR VOLUME MEASUREMENT

Degree for which thesis was presented Grade pour lequel cette thèse fut présentée	Year this degree conferred Année d'obtention de ce grade
MASTER OF SCIENCE	1985
University – Université	**Name of Supervisor – Nom du directeur de thèse**
UNIVERSITY OF ALBERTA	DR. ZOLTAN J. KOLES

AUTHORIZATION – AUTORISATION

Permission is hereby granted to the NATIONAL LIBRARY OF CANADA to **microfilm** this thesis and to **lend** or **sell copies of the film.**

The author reserves other publication rights, and neither the thesis nor extensive extracts from it may be printed or otherwise reproduced without the author's written permission.

L'autorisation est, par la présente, accordée à la BIBLIOTHÈQUE NATIONALE DU CANADA de **microfilmer** cette thèse et de **prêter** ou de **vendre des exemplaires du film.**

L'auteur se réserve les autres droits de publication; ni la thèse ni de longs extraits de celle-ci ne doivent être imprimés ou autrement reproduits sans l'autorisation écrite de l'auteur.

ATTACH FORM TO THESIS – VEUILLEZ JOINDRE CE FORMULAIRE À LA THÈSE

Signature	Date
W J Rutledge	23 APRIL 1985

NL-91 (r. 84/03)

Canada

THE UNIVERSITY OF ALBERTA

AN AIR DISPLACEMENT TECHNIQUE FOR VOLUME MEASUREMENT

by

© WILLIAM JOHN RUTLEDGE

A THESIS

SUBMITTED TO THE FACULTY OF GRADUATE STUDIES AND RESEARCH

IN PARTIAL FULFILMENT OF THE REQUIREMENTS FOR THE DEGREE

OF MASTER OF SCIENCE

DEPARTMENT OF ELECTRICAL ENGINEERING

EDMONTON, ALBERTA

SPRING, 1985

THE UNIVERSITY OF ALBERTA

RELEASE FORM

NAME OF AUTHOR William John Rutledge

NAME OF THESIS An Air Displacement Technique for Volume Measurement

DEGREE FOR WHICH THESIS WAS PRESENTED Master of Science

YEAR THIS DEGREE GRANTED 1985

Permission is hereby granted to THE UNIVERSITY OF ALBERTA LIBRARY to reproduce single copies of this thesis and to lend or sell such copies for private, scholarly or scientific research purposes only.

The author reserves other publication rights, and neither the thesis nor extensive extracts from it may be printed or otherwise reproduced without the author's written permission.

W.J. Rutledge

PERMANENT ADDRESS:

Box 25, Site 18, RR 6

Edmonton, Alberta

T5B 4K3

DATED April 23 1985

THE UNIVERSITY OF ALBERTA

FACULTY OF GRADUATE STUDIES AND RESEARCH

The undersigned certify that they have read, and recommend to the Faculty of Graduate Studies and Research, for acceptance, a thesis entitled

An Air Displacement Technique for Volume Measurement

submitted by William John Rutledge

in partial fulfilment of the requirements for the degree of Master of Science in Engineering.

.....Z. J. Kalés.....
Supervisor

.....

.....

.....

Date ....16 APRIL 1985.....

ABSTRACT

A technique for measurement of incompressible volumes using air displacement is the subject of this thesis. The measurement technique can potentially be used in applications which preclude the use of liquid immersion for volume measurement, notably body volume measurements of infants.

The principal functional components of the equipment are two plexiglass boxes, a motor connected to two pistons, a differential pressure transducer, analog filter electronics and a microprocessor to perform digital filtering, information storage, and polynomial evaluation. The theory, design and construction of the equipment is described in detail.

Results obtained using this equipment to measure the incompressible volume of inanimate and animate objects are presented. The equipment, as built, can resolve incompressible volumes in the range of 0.7 litres to 5.0 litres to 3 per cent. Although the resolution of this equipment is not sufficient for application to infant body volume measurement, the technique appears capable of better resolution. The discussion presents alternative equipment design techniques which could be used to improve the measurement procedure and resolution.

TABLE OF CONTENTS

LIST OF TABLES viii

LIST OF FIGURES ix

CHAPTER I - INTRODUCTION TO BODY COMPOSITION MEASUREMENT 1

Biochemical Measurement Techniques. . . 2

Anthropometric Measurement Techniques . 5

Densitometric Measurement Techniques. . 6

Infant Body Composition 11

Air Displacement Techniques 12

CHAPTER II - THEORY 16

A One-Box Single Stroke System 16

A Two-Box Single Stroke System 19

A Two-Box Oscillating Stroke System . . 22

CHAPTER III - SYSTEM COMPONENTS 27

Boxes 27

Pump 30

Pressure Transducer and Demodulator . . 32

Sampling Wheel and External Trigger Circuitry 33
Output Display and Driver 36

CHAPTER IV - TMS 9900 MICROPROCESSOR 38
Architecture 40
Interrupts 41
Input/Output 42
Texas Instrument Microprocessor Board System 43
Power Supply 43
CPU Board 44
TMS 9901 Programmable Systems Interface 44
TMS 9902 Asynchronous Communications Controller 45
Analog-to-Digital Convertor Board . . . 46
Memory Map 48

CHAPTER V - DIGITAL FILTER DESIGN 50
Digital Filter Basics 50
Design Criteria 53
Filter Derivation 54

CHAPTER VI - ANALOG ANTI-ALIASING FILTER DESIGN 62

CHAPTER VII - RESULTS 67

Frequency Spectrum 67

Calibration Data 69

Measurements of Unknown Volumes 73

CHAPTER VIII - DISCUSSION 77

Box and Pump Characteristics 77

Sinusoidal Amplitude 79

Sinusoidal Phase 81

Leaks 84

Box Expansion 86

Sampling Wheel and Trigger Circuitry . 87

Digital Filter Design 88

Results 88

CHAPTER IX - CONCLUSIONS 96

BIBLIOGRAPHY 99

APPENDIX A 106

LIST OF TABLES

1. Spectral Amplitude Coefficients 25

2. Analog Filter Components 66

3. Unknown Liquid Volume Measurements 74

4. Cat Volume Measurement by Air Displacement 76

LIST OF FIGURES

1.	One-Box Air Displacement System	17
2.	Two-Box Air Displacement System	21
3.	Box Construction	29
4.	External Trigger Circuitry Schematic	35
5.	Output Display and Driver Circuitry Schematic	37
6.	TMS 9900 Microprocessor	39
7.	Memory Map	49
8.	Linear Time-Invariant Discrete Time System	51
9.	Single Precision Integer Format	55
10.	Bandpass Filter - General Amplitude Response	56
11.	Second Order Digital Filter - Canonical Form	61
12.	Two-Pole Analog Filter Schematic	64
13.	System Frequency Response	68
14.	Calibration Curve - Room Temperature	70
15.	Calibration Curve - 30 Degrees Celsius	72

CHAPTER I

INTRODUCTION TO BODY COMPOSITION MEASUREMENT

Determination of the composition of the human body has been an active research topic for over 40 years. With the increasing awareness of the correlation of obesity to atherosclerosis and coronary disease, accurate estimates of body fat are not only helpful in assessing the extent of obesity and the corresponding cardiovascular disease risk factor, but might also yield information related to the effectiveness of the treatment of this condition. The portion of the body that is fat-free, or lean body mass (LBM), has been found to be highly correlated to the energy requirements of the body, and so may be a better index than total body weight for prescribing proper amounts of medication, or for diagnosis of metabolic disorders. As a research tool, the body composition is of great importance in monitoring both normal growth patterns as well as that of patients with specific clinical problems.

The techniques which have been utilized for determination of body composition can be classified into two groups: direct and indirect measurements. Direct measures of fat or lean mass are usually destructive in nature and are confined to carcass analysis. Direct

cadaver analysis has posed a great number of problems and is difficult to perform with great precision. Very few investigations in this area have been performed on human tissue.[1,2] Much more work has been done on laboratory animals but the applicability of the results to human body composition measurement has not been demonstrated.

Indirect measures of body composition take advantage of physical properties of fat and lean tissue to infer their relative proportions. These methods can be applied in vivo and generally fall into three categories: biochemical, anthropometric, and densitometric. These measures will now be discussed in more detail.

Biochemical Measurement Techniques

Biochemical measurement techniques are considered to be inherently more accurate than the other methods, although their potential to be used as an accurate evaluator of other methods has not been taken advantage of to date, largely due to prolonged measurement times.

It has been observed that nitrogen gas dissolves in the body fat in a concentration ratio of five to one over lean body tissue. The nitrogen in lean body tissue is mostly dissolved in body fluids. Thus, breathing a

---

[1]G.E. Pitts, "Studies of Gross Body Composition by Direct Dissection," Annals of the New York Academy of Sciences, 110:11-22, September, 1963.

[2]A. Keys and Jozef Brozek, "Body Fat in Adult Men," Physiological Reviews, 33:345-425, 1953.

pure oxygen atmosphere will wash out dissolved nitrogen over a period of a few hours. The rapid washout from the body fluids can be distinguished from the slower washout from adipose tissue. By measuring the amount of nitrogen released from the body the amount of adipose tissue can be calculated.[3]

A related technique has been used by Lesser et al.[4] It involves measurement of the amount of lipophilic gas that is absorbed by the fat in the body of the subject. This method has the advantage of a higher affinity of these gases to fat than fluid (26:1) as compared to nitrogen above (5:1), and so is more independent of the variations in the composition of fat-free tissue. Disadvantages to both of these methods, though, is the long measurement times involved.

Total body water measurements constitute another major area of body composition research. Normal composition of lean body mass is thought to consist of 73.2% water and adipose tissue contains no water. By determining total body water, the lean body mass can be calculated. The methods of measuring total body water usually involve

---

[3]Albert R. Behnke, "Absorption and Elimination of Gases of the Body in Relation to its Fat and Water Content," Medicine, 24:359, 1945.

[4]Gerson T. Lesser, William Perl and Murray J. Steele, "Determination of Total Body Fat by Absorption of an Inert Gas; Measurements and Results in Normal Human Subjects," Journal of Clinical Investigation, 39:1791-1806, 1960.

isotopic dilution of tracers, such as deuterium oxide.[5] The tracers are substances which are either orally ingested or intravenously injected in fixed quantities, and after an equilibration period the concentration of the tracer in the body fluids is measured. These methods assume equal distribution of the tracer throughout the body fluids. More importantly, however, normal hydration is also assumed and is much more difficult to regulate. In addition, such an invasive procedure is inadvisable for some subjects.

Another biochemical approach is the measurement of the gamma radiation emitted by the naturally occurring radioactive isotope of potassium, ^{40}K, which is found in the the lean mass of the body.[6] This isotope is present in nature in the fixed proportion of 0.012%. Whole body counters have been built to make counts of the gamma radiation of the body from which the total body potassium can be determined and the lean body mass calculated. Although the results show a good correlation to those of the immersion techniques, they are not considered as accurate.

---

[5]Marion J. Stansell and Anthony K. Hyder Jr., "Simplified Body Composition Analysis using Deuterium Dilution and Deuteron Disintegration," Aviation, Space and Environmental Medicine, 47(8):839-845, August, 1976.

[6]G.B. Forbes, J. Gallup and J.B. Hursh, "Estimation of Total Body Fat from Potassium-40 Content," Science, 133:101-102, 1961.

Anthropometric Measurement Techniques

Interest in anthropometric techniques has increased greatly in recent years because they require relatively simple and quick measurements that can easily be performed in a clinician's office. The principle usually involves measurement of circumferences, diameters, or skinfolds at various reference locations of the body. An equation yielding percentage body fat can be obtained by using multiple regression techniques with these measurements as the independent variables, and measures of total body volume, lean body mass, or body fat as determined by other standard techniques as the dependent variables. Equations with exceptionally high correlations and small standard errors of estimate have been derived.[7,8,9] Unfortunately, these equations have shown a specificity to the sampled populations and an equation with general applicability has not been found. Still, it is felt that the ultimate accessibility of body composition measurement as a clinical tool lies with these easily administered techniques.

---

[7]J.H. Wilmore and A.R. Behnke, "Predictability of Lean Body Weight Through Anthropometric Assessment in College Men," Journal of Applied Physiology, 25:349-355, 1968.

[8]J.H. Wilmore and A.R. Behnke, "Anthropometric Estimation of Body Density and Lean Body Weight in Young Women," American Journal of Clinical Nutrition, 23:267-274, 1970.

[9]Arthur Weltman and Victor L. Katch, "A Non-Population-Specific Method for Predicting Total Body Volume and Percent Fat," Human Biology, 50(2):151-158, May, 1978.

Densitometric Measurement Techniques

A number of models of the composition of the human body have been proposed but the most widely accepted is the concept that the body can be divided into two components, one containing fat-free and the other adipose tissue. It is further assumed that these tissues have relatively invariant densities. Investigations that have been made into the variability of the composition of lean body tissue have shown that its relative invariance is sufficient for the applicability of most techniques that have been developed.[10] Knowing the two component densities, as well as the total body density, the proportions of each component can be calculated. Thus most investigations have concentrated on determining total body volume, from which body density can easily be calculated, knowing the body mass.

Body fat is calculated by either the equation derived by Siri[11] or that of Brozek et al[12] which relate body fat to body density. These equations differ only because the values taken as densities of fat and lean body mass were

---

[10]R.J. Wedgwood, "Inconsistency of Lean Body Mass," Annals of the New York Academy of Science, 110:141-152, September, 1963.

[11]W.E. Siri, In: Advances in Biological and Medical Physics. J.H. Lawrence and C.A. Tobial, (eds.) (New York: Academic Press, 1956)

[12]Jozef Brozek, F. Grande, J.T. Anderson and A. Keys, "Densitometric Analysis of Body Composition: Revision of Some Quantitative Assumptions," Annals of the New York Academy of Sciences, 110:113-140, September, 1963.

different in the derivation which follows.

If the two components of total body mass, M_b, are lean body tissue with density D_l, and mass M_l, and fat tissue with density D_f, and mass M_f, then the percentage body fat, $(M_f/M_b \times 100)$, can be calculated as follows:

Total body mass can be expressed as

$$M_l + M_f = M_b$$

Rearranging,

$$1 - \frac{M_f}{M_b} = \frac{M_l}{M_b}$$

Similarly, for total body volume,

$$\frac{M_l}{D_l} + \frac{M_f}{D_f} = \frac{M_b}{D_b}$$

Dividing this equation by M_b, and substituting with the previous equation,

$$\left(\frac{M_f}{M_b} \times \frac{1}{D_f}\right) + \left(1 - \frac{M_f}{M_b}\right) \times \frac{1}{D_l} = \frac{1}{D_b}$$

Rearranging,

$$\frac{M_f}{M_b} \times \left(\frac{1}{D_f} - \frac{1}{D_l}\right) = \frac{1}{D_b} - \frac{1}{D_l}$$

$$\frac{M_f}{M_b} = \frac{1}{D_b} \times \left(\frac{D_f \times D_l}{D_l - D_f}\right) - \frac{D_f}{D_l - D_f}$$

Siri uses $D_f = 0.9$ gm/ml and $D_l = 1.1$ gm/ml. This yields the commonly used equation

$$M_f/M_b = 4.95/D_b - 4.5$$

The two methods most commonly accepted as standards in the evaluation of body composition are derived from Archimedes' Principle. This states that "a solid heavier than a fluid will, if placed in it, descend to the bottom of the fluid and the solid will, when weighed in the fluid, be lighter than its true weight by the weight of the fluid displaced".[13] The volumeter built by Allen involves submerging the subject in a tank of water and measuring the amount by which the water level in the tank has risen.[14] Behnke et al first used the underwater, or hydrostatic, weighing technique to determine body volume.[15] Both of the above methods involve taking measurements quickly during a forced expiration. The residual volume left in the lungs must still be calculated by a nitrogen or helium washout technique.[16,17] Variations in this latter measurement have led to errors in these methods which have been investigated

---

[13] T.H. Heath, The Works of Archimedes (New York: Dover Publications Inc., 1953), p. 258.

[14] Thomas H. Allen, "Measurement of Human Body Fat: A Quantitative Method Suited for Use by Aviation Medical Officers," Aerospace Medicine, 34:907-909, October, 1963.

[15] Albert R. Behnke, B.G. Feen and W.W. Welham, "The Specific Gravity of Healthy Men," Journal of the American Medical Association, 118:495-498, 1942.

[16] T.L. Willman and Albert R. Behnke, "Residual Lung Volume Determination by Methods of Helium Substitution and Volume Expansion," American Journal of Physiology, 153:138-142, April, 1948.

[17] J.H. Wilmore, "A Simplified Method for Determination of Residual Lung Volumes," Journal of Applied Physiology, 27:96-100, July, 1969.

in detail by, among others, Craig and deWare[18] and Girandola et al.[19] Also, any gas in the gastrointestinal tract cannot be measured with these methods. Still, these methods have been taken to be the most accurate of all methods available.

Walser and Stein,[20] and Siri[21] used a method of helium dilution to measure the total body volume. Basically, this method involved mixing a known amount of helium into a compartment containing the subject and which had been calibrated using a number of standards. Measuring the concentration of helium after the mixing and before the helium has had time to diffuse significantly into the tissues would yield a measure of the volume of gas in the compartment including the volume of gas in the subject's lungs. Results from this method have shown a high degree

---

[18] M. Walser and N. Stein, "Determination of Specific Gravity of Intact Animals by Helium Displacement; Comparison with Water Displacement," Proceedings of the Society of Experimental Biology and Medicine, 82:774-777, April, 1953.

[19] W.E. Siri, In: Advances in Biological and Medical Physics J.H. Lawrence and C.A. Tobial, (eds.) (New York: Academic Press, 1956)

[20] S.J. Fomon, R.L. Jensen and J.M. Owen, "Determination of Body Volume of Infants by a Method of Helium Displacement," Annals of the New York Academy of Sciences, 110:80-90, September, 1963.

[21] Albert B. Craig and Donald E. Ware, "Effect of Immersion on Vital Capacity and Residual Volume of the Lungs," Journal of Applied Physiology, 23:423-425, 1967.

of accuracy,[22] and it has the additional advantage of being able to measure infants and elderly or ill patients without the requirement of cooperation by the subject. The reasons why this method has not found much acceptance is not clear. It appears that the only drawback is the need for continual calibration to maintain good accuracy.

There have been other, less popular techniques to measure body or fat volumes. A photogrammetric method of creating a contoured picture of a subject to determine surface area and body volume was developed by Pierson.[23] Soft tissue radiography[24] and ultrasound[25] have been used to measure thicknesses of subcutaneous fat layers. These methods are similar to anthropometric measurement techniques because multiple regression statistics are required to correlate subcutaneous fat to total body fat.

---

[22]Robert N. Girandola, Robert A. Wiswell, John G. Mohler, Gary T. Romero, and William S. Barnes, "Effects of Water Immersion on Lung Volumes: Implications for Body Composition Analysis," Journal of Applied Physiology, 43(2):276-279, August, 1977.

[23]W.R. Pierson, "A Photogrammetric Technique for the Estimation of Surface Area and Volume," Annals of the New York Academy of Sciences, 110:109-112, September, 1963.

[24]Garn, Stanley M. In: Techniques for Measuring Body Composition, Jozef Brozek and Austin Henschel,(eds.), (Washington: National Academy Science and Natural Research Council, 1961) p. 36.

[25]A.W. Sloan, "Estimation of Body Fat in Young Men," Journal of Applied Physiology, 23:311-315, 1967.

Infant Body Composition

In spite of this wealth of research techniques which have been developed, the amount of data which is available concerning the body composition of infants is limited, mostly due to the difficulty in obtaining reproducible estimations of body volume. However, the possible benefits of having such information are quite substantial.

Among the benefits would be the ability to monitor the normal growth pattern of the full term infant. This information could then be compared to the effects of various nutritional regimes for premature infants on their body composition, as well as the growth patterns of infants with specific clinical problems such as: infants who are small for gestational age; infants born to diabetic mothers; and infants with congenital heart disease, severe malnutrition, or large size. At the present time, knowledge in these areas is scanty, largely because of the tremendous technical problems involved, some of which will be described below. What knowledge is available has been derived from indirect and uncalibrated measures such as skinfold measurements and mathematical formulae relating weight and height to body fat or from invasive techniques such as the measurement of body water compartments using isotopes or even body composition by cadaver analysis.

Finally, if a method of measuring the volume of infants is developed with highly reproducible results, then anthropometric techniques may be applied to infants and

their accuracy can be verified by this new "standard".

It is at this point that problems involved with body composition measurements of premature and other young infants surface. Mathematical formulae relating anthropometric measurements to body composition have been shown to be population specific. As such, they may not be applied to infants with any great degree of confidence since confirmation is a difficult task. Immersion techniques are impossible because they require the cooperation of the subject. Invasive techniques such as isotope dilution and radiography are undesirable, if not to the researcher, then to the parents. In fact, the helium dilution method previously mentioned, whole body counting and air displacement techniques are the only methods that have been used with any success.

Air Displacement Techniques

Air displacement techniques have been attempted through most of the last half century, with little success usually due to the difficulties involved with the introduction into the measurement apparatus of a breathing, heat- and moisture-producing infant. Falkner described a method of air-displacement to measure body volume.[26] As expected, after placing the infant in the air-tight box,

---

[26]F. Falkner, "An Air-Displacement Method of Measuring Body Volume in Babies: A Preliminary Communication," Annals of the New York Academy of Sciences, 110:75-79, September, 1963.

the temperature, and hence the pressure, began to increase. The operator would pull a piston out to a preset position, causing a rapid decrease in pressure. This was thought to be an advantage over previous techniques which increased the pressure further by pushing in a piston. By applying Boyle's Law relating the volume and pressure of a fixed amount of ideal gas, the volume of gas in the box, including the lungs and gut could be established. It was found, however, that the systematic errors caused by temperature- and respiratory movement-induced pressure disturbances made the procedure unusable.

Pearse, Scopes and Taylor reported a revision to this air displacement technique which took advantage of some of the technical advances which had been made in the intervening years.[27] It involves the construction of two boxes of identical volume which are connected only through a differential pressure gauge and an adjustable air leak that eliminates slow drifts in the pressure difference due to changes in temperature or humidity. The volumes of both boxes are driven sinusoidally by two pistons connected to the same pump. If the two boxes are empty and the pistons are in phase, no differential pressure signal should be detected. However, if an infant is placed in one of the

---

[27] R. Pearse, J. Scopes, and A. Taylor, "The Measurement of Body Volume in Infants by Air Displacement," Proceedings: Journal of Physiology (London), 256(1):5P, March, 1976.

boxes, an out-of-balance signal should be sensed from which the volume of the infant can be extracted. Pearse et al performed this extraction by a series of analog multiplications by the sine and cosine of the pump frequency, additions, and integrations. Although no quantitative results were cited in their original article, recently published results[28] were reported to be satisfactory and are being used in infant studies. The advantages to such a system for applications such as this include: that it does not require immersion of the infant; it should cause no discomfort to the infant; and it should have no deleterious effect on living tissue.

A similar technique has also been described by Garrow et al.[29] In this case, a two-box differential air displacement technique was being used in conjunction with water displacement. The subject is immersed to the neck, with the head remaining above water. Air displacement is used to determine the volume of the head and lungs.

A two-box air displacement volume measurement similar to that described by Pearse et al is the subject of this thesis. The major modification that has been made in an

---

[28] A. Taylor, Y. Aksoy, J.W. Scopes, G. du Mont and B.A. Taylor, "Development of an Air Displacement Method for Whole Body Volume Measurement of Infants," Journal of Biomedical Engineering, 7:9-17, January, 1985.

[29] J.S. Garrow, R. Diethelm and S.F. Stallex, "An Apparatus for Measuring the Density of Obese Subjects," Journal of Physiology, 267:14P, 1977.

effort to improve the accuracy and flexibility of their design is that the instrument is controlled by a microprocessor. Digitizing the data offers the opportunity for increased accuracy, ease of implementation and flexibility in the range of calculations and analysis possible. It also reduces the need for maintenance, adjustment of some mechanical and analog components, and calibration. Finally, it offers the opportunity for data storage.

CHAPTER II

THEORY

The principles behind a system of volume measurements by air displacement are straightforward. Analysis of such a system requires application of Boyle's Law for an ideal gas plus algebraic manipulations and Fourier analysis.

Boyle's Law states that for a given mass of gas held at a constant temperature, the pressure is inversely proportional to the volume.

$$PV = \text{constant} \tag{1}$$

where P is the absolute pressure and V is the volume of the gas.

A One-Box Single-Stroke System

A closed box of volume, V_B, initially at pressure P_{ATM}, can be compressed in volume by a piston whose stroke volume is V_Δ. Figure 1 shows such a system. In this system, the pressure gauge measures the difference between atmospheric pressure and the pressure within the box. The pressure inside the box will increase during the piston stroke by an amount P_Δ such that

$$P_{ATM}V_B = (P_{ATM} + P_\Delta)(V_B - V_\Delta) \tag{2}$$

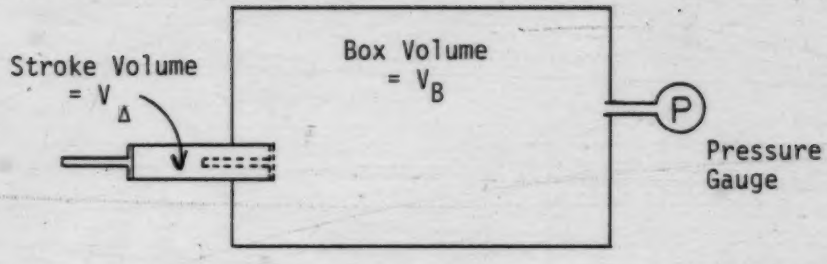

Figure 1. One-Box Air Displacement System

Thus,

$$P_{\Delta} = P_{ATM}\left(\frac{V_{\Delta}}{V_B - V_{\Delta}}\right) \tag{3}$$

If an object of unknown volume, V_x, is put into the box, then when the box is resealed, it has an air volume of $(V_B - V_x)$. If the box is again compressed by V_{Δ}, then the increased pressure is given by

$$P_x = P_{ATM}\left(\frac{V_{\Delta}}{V_B - V_x - V_{\Delta}}\right) \tag{4}$$

If we obtain an expression for P_{ATM} from equation (3) and substitute it into equation (4), the equation becomes

$$P_x = P_{\Delta}\left(\frac{V_B - V_{\Delta}}{V_{\Delta}}\right)\left(\frac{V_{\Delta}}{V_B - V_x - V_{\Delta}}\right) \tag{5}$$

Rearranging,

$$V_x = (V_B - V_{\Delta})\left(\frac{P_x - P_{\Delta}}{P_x}\right) \tag{6}$$

Obviously, the resolution to which we can determine V_x depends on the resolution of the measurement of P_x. By differentiating equation (6) a quantitative expression can be obtained.

$$dV_x = \frac{P_{ATM}V_{\Delta}}{P_x^2}\, dP_x \tag{7}$$

The resolution to which V_x can be determined thus depends on the relative sizes of V_B, V_x, and V_{Δ}.

The following example illustrates the resolution/safety tradeoff in designing a one-box single-stroke system. An instrument is being designed so that children from 0.7 litres volume to 5.0 litres volume could be measured (body weight of 5 kg. or less). To avoid the possibility of any discomfort to the infant due to pressurization of its atmosphere, a maximum pressure limit of +/-1% of atmospheric pressure (assumed to be 760 mmHg) is defined. With 50 litres being a manageable box volume, V_Δ is limited to 0.455 litres. With this stroke volume, it is necessary to use a pressure transducer with an input range of +/-10 mmHg. We will assume that the corresponding transducer output voltage range is +/-10 volts. This voltage can be digitized by a 12-bit A/D convertor. The resolution of the pressure measurement is thus

$$dP_x = 20 \text{ mmHg}/4096 = 0.00477 \text{ mmHg} \qquad (8)$$

From this value and equation (7), the resolution of the volume measurement is calculated to be 2.3 millilitres at V_x = 0.7 litres and this value decreases to 2.0 millilitres at V_x = 5.0 litres.

A Two-Box Single Stroke System

Improving the resolution of the one-box single stroke system is possible by increasing the pressure in the box by more than 1% of atmospheric pressure or increasing the resolution of the pressure measurement. The former may

cause discomfort or injury to the infant and cannot be considered. The latter is possible by increasing the digit resolution of the A/D convertor or by constructing a two-box single stroke system as shown in figure 2. In effect, the measurements of P_x and P_Δ which were performed on one box, are performed simultaneously in one measurement. In this system, the differential pressure transducer responds to P_m, the difference between the pressures in the boxes. The transducer no longer has to resolve small pressure changes in a large dynamic range, and the resolution is thereby improved.

In terms of the single box system,

$$P_m = P_x - P_\Delta \tag{9}$$

By substituting expressions in equations (3) and (4) into (9) above,

$$P_m = \left(\frac{P_{ATM} V_x V_\Delta}{V_B - V_\Delta}\right)\left(\frac{1}{V_B - V_x - V_\Delta}\right) \tag{10}$$

Rearranging,

$$V_x = \frac{V_B - V_\Delta}{\frac{P_{ATM}}{P_m}\left(\frac{V_\Delta}{V_B - V_\Delta}\right) + 1} \tag{11}$$

The resolution of this system is now given by

$$dV_x = \frac{P_{ATM} V_\Delta}{\left(\frac{P_{ATM} V_\Delta}{V_B - V_\Delta} + P_m\right)^2} dP_m \tag{12}$$

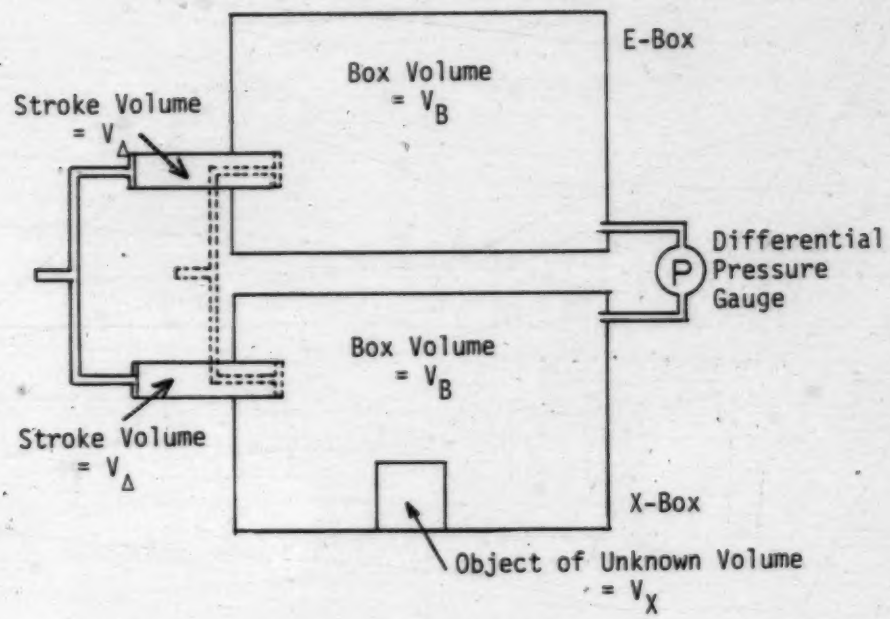

Figure 2. Two-Box Air Displacement System

Calculation of the resolution of this system can again be illustrated using an example. The maximum pressure excursion is again chosen to be +/-1% of atmospheric pressure, but the stroke volume has been changed to 0.70 litres. The transducer now has an input range of +/-0.525 mmHg and output of +/-10 volts. All other specifications are identical to those given in the previous example. The resolution of the pressure measurement is thus,

$$dP_m = 1.050 \text{ mmHg}/4096 = 0.000250 \text{ mmHg} \qquad (13)$$

The resolution of volume measurement at V_x = 0.7 litres is improved to 0.22 millilitres. At V_x = 5.0 litres, the resolution is 0.19 millilitres.

A Two-Box Oscillating Stroke System

There are difficulties inherent with a single stroke system, however. An infant placed in a sealed box will tend to increase both the temperature and humidity of the air inside the box. These increases will be observed as a rise in the differential pressure over the measurement period. In addition, breathing and perhaps movement will produce small changes in the pressure within the box at low frequencies. In the two single stroke systems previously described, measurement of these effects and elimination of their contribution to a pressure measurement is difficult.

A system in which the stroke volume oscillates at a constant frequency can avoid most of this systematic error. The output pressure signal is bandpass filtered so that only the component at the stroke frequency is measured. Low frequency effects of temperature change or breathing are attenuated, as are high frequency effects associated with impulse pressure changes. As will be seen in the analysis that follows, however, there is no significant loss in precision.

Using the same two box system as in figure 2 and applying sinusoidal volume changes of angular frequency ω, equation (14) describes the pressure in the empty box.

$$P_{ATM}V_B = P_{\Delta E}(t)(V_B - V_\Delta \sin\omega t) \qquad (14)$$

In the other box, which contains an object of incompressible volume, V_x,

$$P_{ATM}(V_B - V_x) = P_{\Delta x}(t)(V_B - V_x - V_\Delta \sin\omega t) \qquad (15)$$

The measured differential pressure signal thus becomes

$$P_m(t) = P_{\Delta x}(t) - P_{\Delta E}(t)$$

$$= P_{ATM}\left(\frac{V_B - V_x}{V_B - V_x - V_\Delta \sin\omega t} - \frac{V_B}{V_B - V_\Delta \sin\omega t}\right) \qquad (16)$$

Rearranging,

$$P_m(t) = P_{ATM}V_\Delta V_x\left(\frac{\sin\omega t}{V_B(V_B - V_x) - V_\Delta(2V_B - V_x)\sin\omega t + V_\Delta^2 \sin^2\omega t}\right) \qquad (17)$$

The expression is periodic with period, $T=2\pi/\omega$, and is an odd function since $P_m(t) = P_m(-t)$. Because of these properties, it has a Fourier sine series expansion

$$P_m(t) = \sum_{n=1}^{\infty} b_n \sin(n\,t) \qquad (18)$$

where the coefficients b_n are given by

$$b_n = \frac{2\omega}{\pi}\int_0^{\pi/\omega} P_m(t)\sin(n\omega t)\,dt \qquad (19)$$

The b_n are obviously functions of V_B, V_Δ, and most importantly, V_x .

For any system of this sort, the volumes V_B and V_Δ will be fixed as constants. As a result, calculation of b_n as a function of V_x is performed based on the specifications given in previous examples, namely V_B = 50 litres and V_Δ = 0.70 litres. For each harmonic, n, numerical integration using Simpson's Rule is performed to find b_n values for 1435 points within the range {0.7 litres $\leq V_x \leq$ 5.0 litres}.

The 1435 points form a curve which is fitted by the least squares method to a polynomial of degree 3. The coefficients that result are listed in table 1. The fundamental frequency yields the largest amplitude signal, slightly larger than the DC component, but more than 4 orders of magnitude greater than the second harmonic.

TABLE 1

SPECTRAL AMPLITUDE COEFFICIENTS

	$[*v_x^0]$	$[*v_x^1]$	$[*v_x^2]$	$[*v_x^3]$
Degree	0	1	2	3
Spectral Amplitude				
b_0 $(*10^{-2})$	-0.00164	6.85	0.135	0.00336
b_1 $(*10^{-2})$	-0.00437	10.78	0.212	0.00541
b_2 $(*10^{-6})$	-2.17	1.39	-1.49	0.476

Over the dynamic range of the system, the cubic term contributes a maximum of less than 0.1% to the amplitude and so is neglected.

Thus the first harmonic amplitude can be approximated over the range {0.7 litres $\leq V_x \leq$ 5.0 litres} as

$$P_{m1}(V_x) = (-0.00437 + 10.78V_x + 0.212V_x^2) \times 10^{-2} \qquad (20)$$

The resolution of this measurement is thus obtained as

$$dV_x = \frac{100}{10.78 + .414V_x} \, dP_{m1} \qquad (21)$$

At V_x = 0.7 litres, the resolution in the volume measurement is 2.3 millilitres and at V_x = 5.0 litres, the precision is 2.0 millilitres. In this example, a two-box oscillating stroke system was assumed to be constructed using a pressure transducer and demodulator for which dP_x is defined by equation 13. There is no significant loss of resolution when compared to a single stroke system. This system design does eliminate some systematic error, however.

CHAPTER III

SYSTEM COMPONENTS

Boxes

Two custom made plexiglass boxes are the principal mechanical components of the system. They are constructed of 9.5 mm. plexiglass to allow observation of infants placed inside the boxes. Approximate internal dimensions of 16 cm. X 35 cm. X 31.5 cm. provide a volume of about 50 litres in each box.

The tops of both boxes are fitted with tapered brass bulkhead connectors for 4.8 mm. flexible tubing. A short length of tubing is attached to the fittings on each box to form the slow leak necessary for elimination of very low frequency pressure differentials due to temperature or humidity changes. Both boxes have an 8.3 cm. diameter hole in one side, with a short length of plexiglass tubing extending from the hole. This tubing serves as a flange to which the hose from the pistons can be clamped.

The two boxes are mounted with screws onto a 43 cm. X 114 cm. sheet of 15.9 mm. plywood. A gap of about 8 cm. is left between the boxes to allow mounting of the pressure transducer between them. The brass connectors fitted on the boxes which hold the pressure transducer

rigidly in place are 3.2 mm. inner diameter. By mounting the boxes in this way, they cannot be moved relative to one another. The pressure transducer and fittings are not designed to tolerate the mechanical stresses which could have resulted from only one box being moved.

The boxes are not entirely identical, however. To distinguish the two boxes in the following descriptions, the box which is used to contain the unknown volume will be designated X-box, while the box which remains empty will be designated E-box.

The top of X-box is the lid which is opened for insertion and removal of the object with unknown volume. The box is sealed by clamping an aluminum ridge on the lid into a soft rubber gasket on the box. The lid's piano hinge is fully compressed when the lid is closed and the four clamps shown in figure 3 are tightened. A good seal is also ensured by spreading silicone lubricant over the gasket.

The top of E-box, although not hinged, is removable. It is held in place by 20 wing nuts which tighten the top to the box. Having this removable top allowed modifications to be easily made to both the top and the remainder of the box. The top of E-box is fitted with a piston for fine adjustments in box volume. The piston is made from 4.8 mm. plexiglass tubing with a 10.2 cm. inner diameter. The piston head is sealed with an o-ring and actuated by a screw threaded with 12.6 threads per

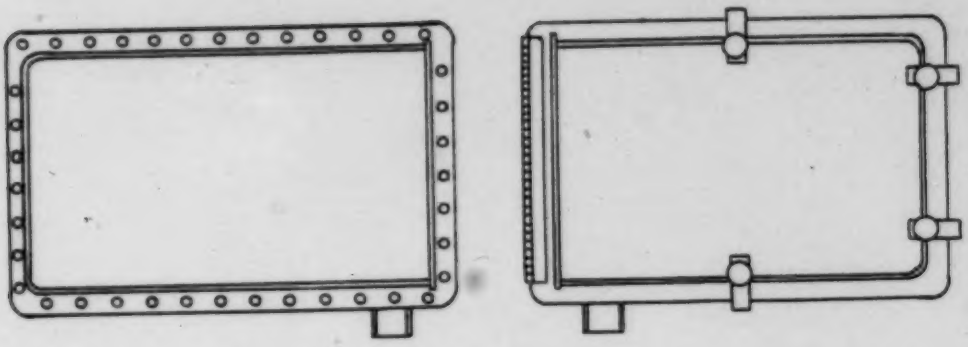

TOP VIEW

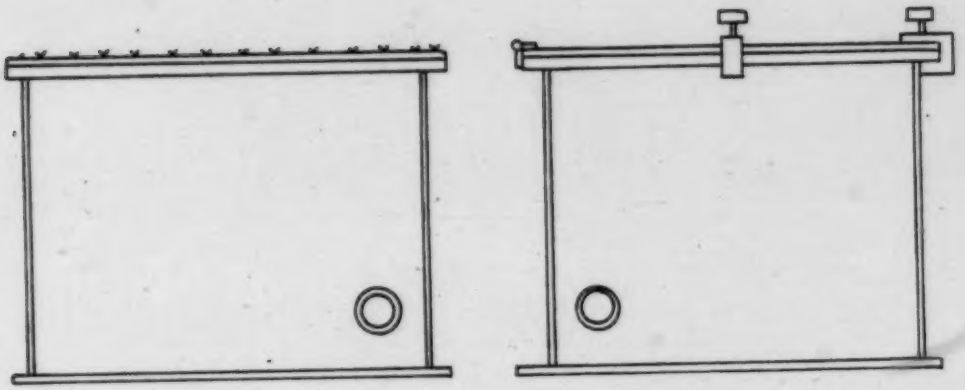

SIDE VIEW

Figure 3. Box Construction

centimeter. This assembly permits volume adjustments of over 1 litre. One full turn of the screw, however, only changes the volume by about four millilitres.

Pump

The pump which supplies an oscillating stroke volume is a Harvard Apparatus model #614 dog respirator. When operated as a respirator, a 1/15 HP gear head motor turns a slotted crank to which a 8.3 cm. diameter piston has been attached. The respirator has controls which enable the user not only to vary the stroke rate from 5 to 50 strokes per minute, but also to independently vary the inspiratory and expiratory times as well. The stroke volume can also be set from 0 to 700 ml. by adjusting the point of attachment of the piston rod along the crank. For this application, the stroke volume was set to 700 ml. and the stroke rate was set at the maximum rate of approximately 0.9 hertz.

This basic respirator has been modified in three ways to perform the requirements of this application. First, an additional crank and piston assembly has been attached to the motor shaft. This modification permits volume oscillations in two independent air reservoirs. However, the relative phase between the two piston cycles remains constant while the motor speed is changed. One of the two cranks is screw-tightened to the motor shaft. This permits adjustment of the relative phase between the two piston

cycles.

The second modification to the basic respirator involved removing an eccentric cam on the motor shaft. This cam had actuated a switch which is used in the independent adjustment of inspiratory and expiratory times. With this switch inactive, the inspiratory and expiratory times are both 50% of the total cycle time.

Finally, a piston cylinder is normally fitted with two one-way valves: one valve allows external air into the cylinders as the piston rod is retracted and the other valve allows air out to the animal as the piston rod is extended. For the present application, however, there is only one reservoir of air per piston. Each box both provides air as the piston rod is retracted and accepts air as the piston rod is extended. The piston head is, in effect, a "wall" of the air reservoir which can move in and out in approximately sinusoidal motion.

Therefore, the two one-way valves and the orifices they are set in are not required and only add resistance to air flow to and from the cylinders. The endplates of each of the pistons were removed, permitting free flow of air in and out of the cylinder.

Twenty centimetre lengths of flexible steel-reinforced 8.9 cm. hose connect each piston to a box. Hose clamps hold the hose in place at either end. The outside of the piston cylinders and box flanges were greased to completely seal each connection.

Pressure Transducer and Demodulator

A Validyne DP103-871 differential pressure transducer and Validyne CD12-871 carrier demodulator was purchased for this application. The most outstanding feature of these components was their ability to produce a full-scale +/-10 volt DC output for a differential input pressure of +/-1.050 mmHg. Other features of these components which are relevant to this application will be discussed in the following detailed description. The pressure transducer consists of a very thin, magnetically permeable stainless steel diaphragm held between two blocks. The very small cavities on either side of the diaphragm are pressurized through ports in the transducer housing. A pressure difference between the ports causes the diaphragm to move from its undeflected position.

Imbedded in each of the two blocks holding the diaphragm are an E-core and coil assembly. The lines of magnetic flux through the energized coils must cross the gap between the E-core and the magnetically permeable diaphragm. Deflection of the diaphragm increased the gap for one coil and decreases the gap for the opposite coil. Correspondingly, the inductance of the first coil decreases and that of the second coil increases as the flux through coils changes.

The two coils form two arms of a bridge circuit which is excited by a 5 KHz, 5 volt RMS sinusoidal signal supplied by the carrier demodulator unit. Changes in coil

inductances change their impedance, and the amplitude of the bridge circuit output is therefore proportional to the transducer imbalance. The carrier demodulator amplifies, rectifies and then filters the signal to produce a DC output.

The transducer is linear within a +/-0.5% of full scale from a "best" straight line. It will withstand an overpressure of +/-200% of full scale with less than 0.5% of full scale zero shift.

The carrier demodulator will supply a full scale output with a minimum sensitivity of 15 mV output per volt of excitation. This input sensitivity is also adjustable by a span control vernier. Finally, the frequency response of the demodulator can be set to one of four ranges from 0-10 Hz. to 0-1000 Hz.

Sampling Wheel and External Trigger Circuitry

A 6.35 cm. diameter wheel was constructed of opaque black plastic with sixteen 1.6 mm. wide slots cut at equal intervals around the circumference. The angles between consecutive slots were measured to be within 1% of 22.5°. The wheel was mounted on the motor shaft between the crank and the gear housing.

A General Instrument MCT 81 slotted optical limit switch was also mounted on the gear housing so that the wheel edge passes through the gap in the limit switch. The limit switch operates by transmitting light from a GaAs

infrared emitting diode to a silicon phototransistor. Both semiconductor chips face each other across a 2.54 mm. wide gap and the MCT 81 senses an object in the gap by the interruption of light transmission.

The pulse produced as a slot in the wheel passes through the limit switch gap is large enough to switch a TTL load but is not fast enough to meet the requirements of the A/D external convert command. The specification for this signal is an active-low TTL-level pulse from 200 to 1000 nanoseconds duration. As a result, a circuit to speed up the trigger pulse from the limit switch was constructed on the prototype board. The schematic for this circuit is shown in figure 4.

The Schmitt trigger (U1) speeds up the pulse edges of the emitter follower output from the phototransistor. A 10K resistor sets the threshold hysteresis at about 0.2 volts. Since the pulses occur 16 times per piston cycle and the desired sampling interval is 8 times per piston cycle, the pulse train frequency is divided by 2 by a counter (U2). A buffer (U3) interfaces the preceding CMOS circuitry with a TTL monostable (U4). The monostable produces a negative-going pulse of duration 400 nanoseconds on a falling edge of the input pulse train. It is this monostable output pulse that triggers an external convert command on the A/D convertor board.

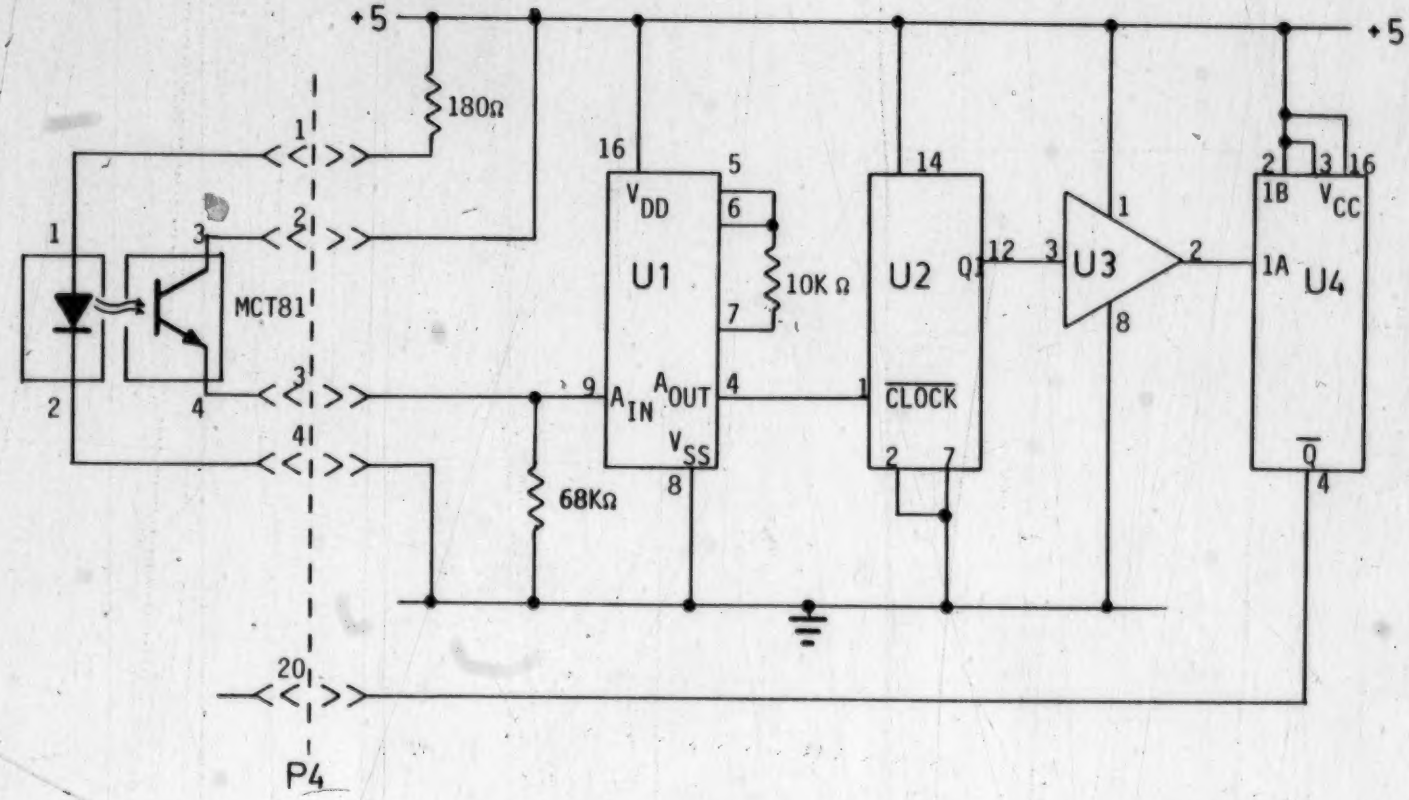

Figure 4. External Trigger Circuitry Schematic

Output Display and Driver

The final peripheral equipment requirement for this application was a display for monitoring the performance of tasks by the microprocessor as well as outputting the final result.

Since it was expected that the maximum precision to which a measurement could be made would be 0.1%, a 4-digit display was required. The ambient environment of the instrument is well-lit so an AND model FE0202 field effect liquid crystal diode (LCD) display was purchased. This display featured four 12.7 mm. high digits, 3 decimal points and a colon. The package included connector pins at standard 2.54 mm. spacings.

An Intersil ICM7211M LCD display decoder/driver was purchased for interfacing the microprocessor with the display. This IC supplies 4 digit non-multiplexed 7-segment display outputs. It also contains an RC oscillator to generate the backplane frequency required by the LCD display. Data input latches and digit select code latches under the control of high-speed chip select inputs simplify the interface with a microprocessor. Extra read only memory or CPU time for decoding and display updating is not required.

Figure 5 shows the schematic of the display and driver circuit.

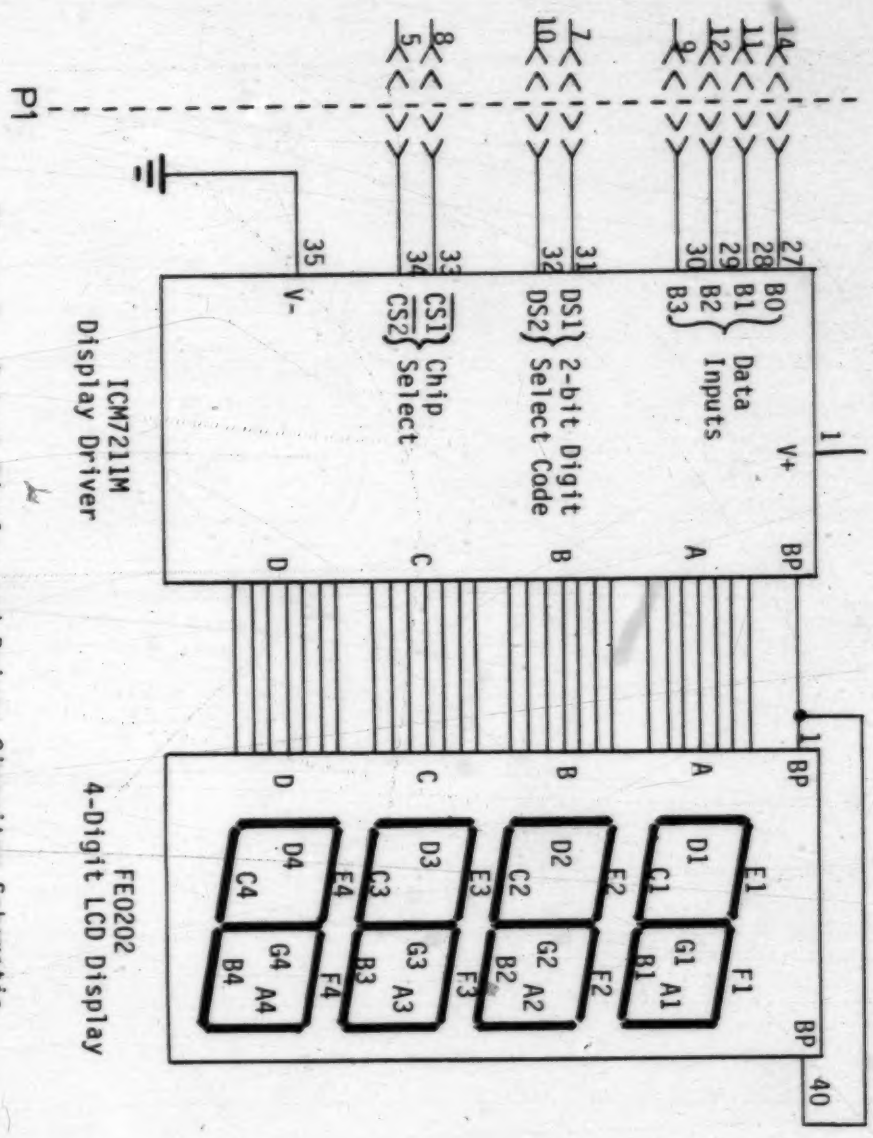

Figure 5. Output Display and Driver Circuitry Schematic

CHAPTER IV

TMS 9900 MICROPROCESSOR

The Texas Instruments TMS 9900 is one of a large number of single chip 16-bit microprocessors available. It is implemented using N-channel silicon gate MOS technology in a 64-pin package (See figure 6).

An introduction to the terminology, characteristics and applications of microprocessors can be found in many textbooks[1,2] and will not be discussed here. In addition, particular details concerning the theory of operation and the instruction set of the TMS 9900 can be found in a number of Texas Instrument publications which will be cited as each component is briefly discussed below. However, there are a number of features of the TMS 9900 which are relatively uncommon and which influence the present design. The description of these features which follows should contribute to understanding of the present system and program design.

---

[1]John P. Hayes, Computer Architecture and Organization, New York: McGraw Hill Book Company, 1978.

[2]William D. Simpson, Gerald Lueckee, Don L. Cannon, and David Clemens, 9900 Family Systems Design and Data Book, Houston: Texas Instruments Incorporated, 1978.

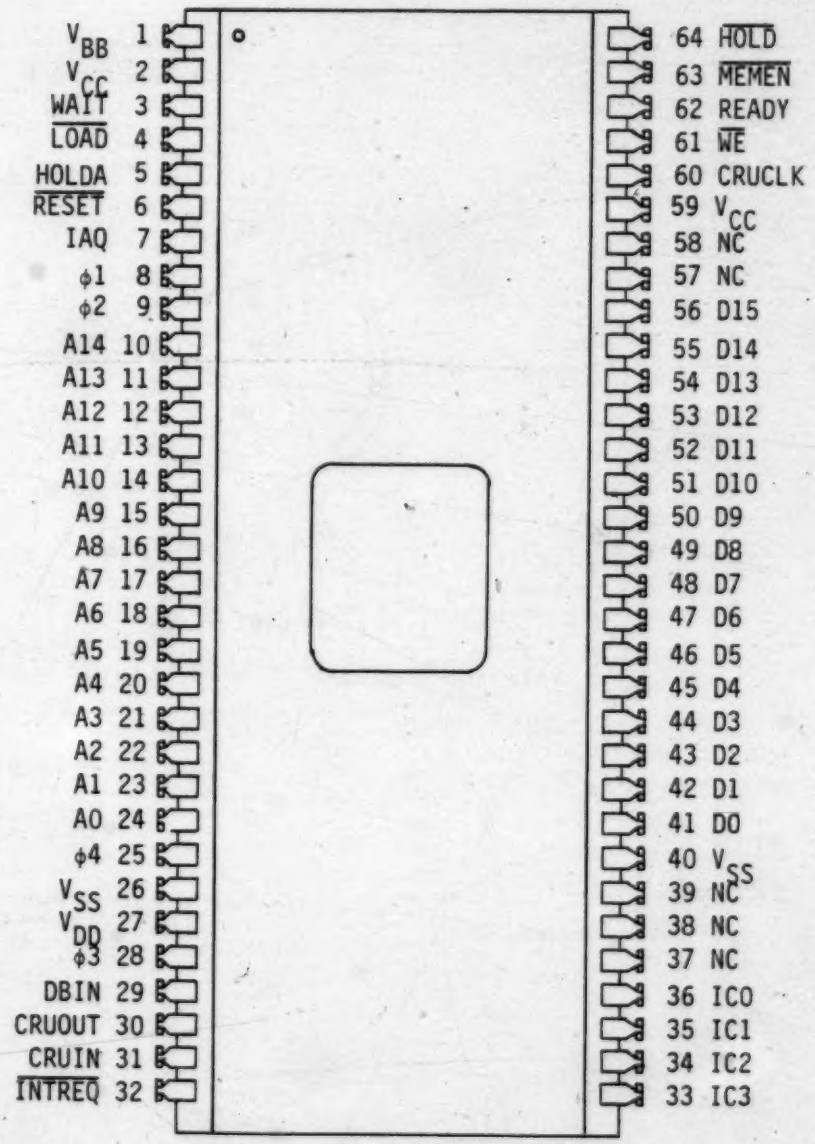

Figure 6. TMS 9900 Microprocessor

Architecture[3]

The primary feature of the TMS 9900 architecture is its ability to locate register files in any available area of random access memory. Texas Instruments uses the term "memory-to-memory" to describe this architecture. The register files contain 16 general-purpose 16-bit registers which are located in a block of 32 contiguous bytes of memory. Such a block is called the workspace.

Each of these 16 registers can contain operands, or can be used as an accumulator, address or index register. Most instructions operate on these registers in addition to the CPU's internal registers, of which only the following 3 are accessible to the user:

1. the program counter (PC) which contains the address of the program instruction following the current instruction being executed.
2. the status register (ST) which contains the processor's interrupt mask and other information relevant to the operation and operands.
3. the workspace pointer (WP) which contains the address of the first byte in the current workspace.

The first two registers are common to most microprocessors. However, the workspace pointer is used to access the general purpose registers by adding their

---

[3]Texas Instruments Incorporated Semiconductor Group, TMS 9900 Microprocessor Data Manual, Houston: Texas Instruments Incorporated, 1978.

numerical designation (binary representation) of 0 to 15 to the WP. By performing a context switch, a new address is inserted into the WP, accessing a new set of 16 registers. This feature is especially convenient for writing programs containing subroutines. Instead of using a stack to store the WP, PC, and ST of the calling routine, the BRANCH AND LOAD WORKSPACE POINTER (BLWP)[4] instruction stores these numbers in registers 13, 14 and 15 of the new subroutine's workspace. This also facilitates nesting of subroutines.

Interrupts

The TMS 9900 is designed for fast interrupt handling, in part, by having a separate interrupt bus. It has 16 interrupt levels arranged in descending priority: highest priority being level 0 and lowest priority being level 15. An interrupt mask is contained in bits 12 to 15 of the status register. When an interrupt request is received on ~INTREQ, the 4-bit priority level of the interrupt is read on pins IC0 to IC3 and compared to the interrupt mask. For interrupts with priority levels equal to or less than the mask value, the interrupt is recognized, and a context switch to the interrupt service routine is performed. The jump to the service routine is like a BLWP instruction to

---

[4]Texas Instruments Incorporated Semiconductor Group, Model 990 Computer/TMS 9900 Microprocessor Assembly Language Programmer's Guide, Houston: Texas Instruments Incorporated, 1978.

the appropriate interrupt vector location, except that the interrupt mask is set to a value one less than the priority level of the interrupt being serviced. This prevents subsequent interrupts with a lower priority. A RETURN WORKSPACE POINTER (RTWP) instruction concludes the interrupt servicing routine by returning the WP, PC, and ST registers to the values they held at the time the interrupt was recognized.

Input/Output

Input to and output from the TMS 9900 is performed through a command driven interface called a communications register unit (CRU). The CRU provides up to 4096 directly addressable bits which can be assigned as either input or output. Depending on their assignment, individual bits may be set, reset or tested. Alternatively, information can be serially loaded to and from the CRU, for external access in fields from 1 to 16 bits.

As was the case for interrupt handling, I/O is made faster with dedicated pins: in this case, there are three. Data is fed out through CRUOUT, fed in through CRUIN, and CRUCLK is a control line which, if high, indicates an output transfer. The destination or source address of an I/O transfer or test is calculated as a displacement from the CRU base address which is found in 12 bits, 3 to 14, of register 12 of the current workspace. This address is placed on the address bus to select the I/O device. The

displacement used in calculation of this address is contained in bits 8 to 15 of the instruction and allows two's complement addressing of CRU bits from base minus 128 through base plus 127.

Texas Instrument Microprocessor Board System

In an effort to minimize the microprocessor system development time, it was decided to purchase a TMS 9900-based microprocessor board system marketed by Texas Instrument's Semiconductor Division. The purchased system included a TM990/518A power supply, a TM990/510A 4-slot card cage, a CPU board, an analog-to-digital convertor board, and a wirewrap prototype board. Descriptions and specifications of these components are contained in the following subsections.

Power Supply

The TM990/518A power supply provides all the voltages required by the TMS 9900-based microprocessor board system. It has the capability to supply +5 volts at 4.0 amperes, +12 volts at 0.6 amperes and -12 volts at 0.4 amperes. An additional voltage of +45 volts at 0.1 amperes is provided for user's circuits but was not used in this application. The power supply is mounted in a metal box with an ON/OFF switch and red LED indicating power on. It is connected to the card cage via a multiconductor cable with spade terminals.

CPU Board

The CPU board contains all the basic components sufficient for operation of a basic microprocessor system, except for a power supply. It includes a TMS 9900 microprocessor, a TIM 9904 clock generator (SN74LS362), 1 kilobyte of random access memory (capacity for 4KB), and 2 kilobytes of static read-only memory (capacity for 8KB). Also included are two I/O peripheral devices: a TMS 9901 programmable systems interface and a TMS 9902 asynchronous communications controller.

TMS 9901 Programmable Systems Interface[5]

The TMS 9901 programmable systems interface (PSI) is designed for interfacing the TMS 9900 microprocessor chip with up to 22 external interrupt and I/O ports. Six of the ports are dedicated as interrupt inputs, seven ports are dedicated as either input or output ports, and 9 ports can be programmed as interrupt or I/O ports. The TMS 9901 generates the interrupt code for the priority of the interrupt port, as well as generating the ~INTREQ signal. In addition, the 3 CRU lines are used by the chip's I/O control logic to handle the I/O ports. Outputs on the 9901 are latched until they are reset.

---

[5]Texas Instruments Incorporated Semiconductor Group, TMS 9901 Programmable Systems Interface, Houston: Texas Instruments Incorporated, 1978.

TMS 9902 Asynchronous Communications Controller[6]

The TMS 9902 Asynchronous Communications Controller (ACC) is designed to provide an interface between a microprocessor and a serial, asynchronous, communications channel. The ACC performs the timing and data serialization and deserialization functions, and features the ability to program I/O character length, number of stop bits, parity, and data transfer rate. The asynchronous communications controller included on on the CPU board is used in this application for asynchronous communications with a Viewpoint terminal. It is configured by the program for RS232 asynchronous communications at 9600 baud rate, odd parity, seven-bit character length, and 1 stop bit.

The communications are handled using Extended Operation (XOP) instructions. These instructions can be thought of as functions whose workspace pointer and program counter are stored at predefined addresses between 40_{16} and $7F_{16}$. Up to 16 XOP instructions can be defined. Execution of an XOP instruction involves obtaining the WP and PC from the location corresponding to the XOP instruction (0 to 15) and storing the source address and old WP, PC, and ST in the new workspace.

---

[6]Texas Instruments Incorporated Semiconductor Group, TMS 9902 Programmable Systems Interface, Houston: Texas Instruments Incorporated, 1978.

Four XOP instructions are used to handle asynchronous communications:

XOP 0 -- initiating communications with Viewpoint terminal

XOP 1 -- receiving characters from terminal

XOP 2 -- sending characters to terminal

XOP 3 -- test to see if previous I/O request is complete

Interrupt level 4 is generated by the communications controller to indicate that the transmit buffer is empty or that the receiver buffer is full. The XOP instructions handle the movement of characters to and from the buffers.

Analog-to-Digital Convertor Board[7]

The heart of the analog-to-digital (A/D) convertor board is an Analog Devices RTI-1240 A/D convertor. An Analog Devices 0A09 DC-DC Power Convertor provides reference voltages on the board. The A/D convertor can access up to 16 differential or 32 single-ended inputs. The voltage is resolved to 12 bits.

The board provides a number of options for the user. The voltage range for full scale output can be selected to be +/-10V, +/-5V, 0V to 10V, or 0V to 5V. Further gain adjustment can be made by resistor replacement. Output can be obtained as simple magnitude or two's complement

---

[7]Analog Devices Instruments and Systems. RTI-1240/1241 User's Reference Manual, Norwood, Massachussetts: Analog Devices Inc.

formats. The voltage ranges and output formats can be selected by on board jumpers. The A/D convertor board is equipped for TMS 9900 compatible interrupt generation with interrupt priority level also being jumper selectable. The final option selected by jumpers on this board is the base address (BASE) location of the A/D convertor access words in the microprocessor memory map. These 8 access words are memory mapped instead of using the CRU for data transfer as in other I/O described in this application.

There are a number of options that are selected by setting or resetting bits in these access words, which are treated by the CPU like any other RAM location to be written into or read from. The word at BASE+4 is used to select options: whether or not an external pulse will trigger a conversion, whether or not an interrupt will be generated upon completion of the conversion and whether or not sampling will be multiplexed through the 16 channels by automatically incrementing the channel select number. Only the first two of these options were used used in this application. The word at BASE+8 selects the channel to be sampled. The word at BASE+10 is written into for software initiated conversions. The word at BASE+12 contains the status of the conversion. That is, if bit 2 is 1, the conversion is still underway, and if it is 0, the conversion is complete. The status word must be read to reset this bit before a subsequent conversion can take place. Finally, the word at BASE+14 contains the output

data after the conversion is complete, in whatever format had been selected.

Memory Map

Figure 7 shows the memory map for the present application. The flowchart of the program shown in appendix A.

There are only three active interrupts. Interrupt level 0 is RESET, activated by a switch on the CPU board. This switch performs the function of a restart. Interrupt level 1 is an A/D conversion complete signal initiated by the A/D convertor board. Interrupt level 4 is generated by the 9902 asynchronous communications controller to indicate that input or output of terminal information has been completed.

Memory Type	Area Definition	Memory Address (Base 16)	Memory Content	Function
ROM	Interrupt Vectors	0000 0002	WP Level 0 Interrupt PC Level 0 Interrupt	Reset
		0004 0006	WP Level 1 Interrupt PC Level 1 Interrupt	End of Conversion
		0010 0012	WP Level 4 Interrupt PC Level 4 Interrupt	Terminal I/O
	XOP Software Trap Vectors	0040 0042	WP XOP 0 PC XOP 0	Initialize Terminal I/O
		0044 0046	WP XOP 1 PC XOP 1	Initiate Read from Terminal
		0048 004A	WP XOP 2 PC XOP 2	Initiate Write to Terminal
		004C 004E	WP XOP 3 PC XOP 3	Check if Terminal I/O Complete
	Program and Constants	0080 1FFF		
N/A	Mapped I/O for A/D Convertor	AFF0 AFFF		
RAM	Workspace Registers and Variables	FC00 FFFB		
	Load Signal Vector	FFFC FFFE	WP Load Function PC Load Function	

Figure 7. Memory Map

CHAPTER V

DIGITAL FILTER DESIGN

The principles of digital filter design can be found in many textbooks and current articles. The following should only serve as a brief background for the reader.

Digital Filter Basics

A linear time-invariant discrete time system is shown symbolically in figure 8. The input $\{x_n\}$ is a sequence of numbers where n may be finite or infinite. Of course, in digital systems realized by computer, each x_n is truncated at a finite number of digits and n is also finite. The output sequence is related to the input by the impulse response of the system $\{h_n\}$. The latter sequence is so named because it can be found by determining the response of the system to a unit impulse input signal at n=0.

$$\left.\begin{aligned} x_n &= 0, \quad n \neq 0 \\ x_n &= 1, \quad n = 0 \end{aligned}\right\} \tag{22}$$

The system of figure 8 can then be described by equation 23.

$$y_n = \sum_{i=-\infty}^{\infty} x_i h_{n-i} \tag{23}$$

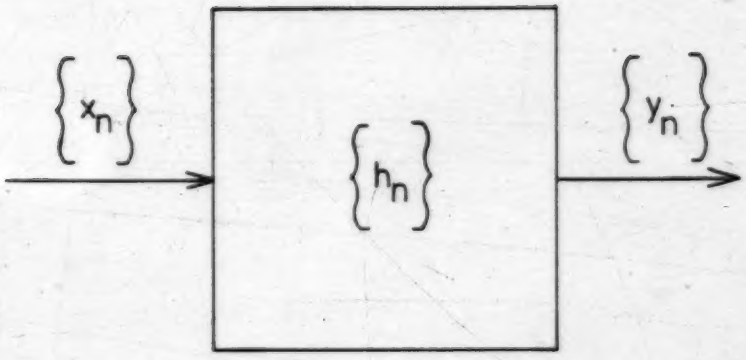

Figure 8. Linear Time-Invariant Discrete Time System

where $\{y_n\}$ is a convolution of $\{x_n\}$ and $\{h_n\}$. From the convolution properties of the z-transform, equation 23 becomes

$$Y(z) = H(z)X(z) \tag{24}$$

where F(z) is the z-transform of a sequence $\{f_n\}$ defined as follows

$$F(z) = \sum_{n=-\infty}^{\infty} f_n z^{-n} \tag{25}$$

A large class of linear time invariant systems can be described by the linear constant coefficient difference equation.

$$y_n = \sum_{k=0}^{M} a_k x_{n-k} - \sum_{k=1}^{L} b_k y_{n-k} \tag{26}$$

By taking z-transforms of this equation, it can be written as

$$Y(z) = \left(\frac{\sum_{k=0}^{M} a_k z^{-k}}{1 + \sum_{k=1}^{L} b_k z^{-k}} \right) X(z) \tag{27}$$

The quantity in brackets above is the transfer function of the filter, H(z), of equation 24. Designing a digital filter requires selection of appropriate coefficients $\{a_k\}$ and $\{b_k\}$ to produce the desired effect on the signal.

Design Criteria

There are two classes of digital filters. If all the b_k in equation 27 are zero, then the transfer function reduces to a polynomial in z and results in a non-recursive finite impulse response (FIR) filter. If at least one b_k does not equal zero, then the filter is recursive and has an infinite impulse response (IIR). Each of these classes can be found to be more suitable than the other, depending on the application.

In the present case, it is known that the sampling pulse is generated by a slotted wheel, mounted on the pump shaft, interrupting light which gates a phototransistor. Because of mechanical tolerances in the production of this wheel, it was found that the sampling rate varied +/-2 percent. To select only the frequency component at the pump frequency, a narrow passband was required. But to avoid uneven attenuation as the sampling rate varied, a maximally flat passband filter was needed.

One realization of such a filter was as an IIR filter. Using analog filter design methods to obtain the transfer function of an analog filter, the digital filter transfer function is obtained by transforming the Laplace transform variable, s, to the z-transform variable, z. In this way, the analog frequency response is mapped into a desired digital frequency response. Computer realization of such a digital filter, however, required floating point arithmetic subroutines to perform the single precision operations

(24-bit mantissa, 8-bit exponent - See Figure 9). These subroutines will not be listed in this thesis, but they were written using the algorithms used by Hewlett Packard on their 2100 series computers.

Filter Derivation

The following derivation of the digital filter follows the method described by Peled and Liu in chapter 2 of "Digital Signal Processing: Theory, Design and Implementation".[1] This method involves selection of an analog low pass filter and applying a transformation to the analog transfer function to obtain the desired digital transfer function, H(z). In particular, bilinear transformations between the complex variables s and z are used to map the poles and zeroes in the left half of the s-plane to the interior of the unit circle $|z|=1$. The analog frequency response in the semi-infinite interval, $0 < \omega < \infty$, to a digital frequency response in the interval, $0 < \lambda < \pi$.

A general amplitude response of a digital bandpass filter is shown in figure 10 in order to indicate labels which will be used in the following derivation. The frequencies $\Lambda_{PL} \leq \lambda \leq \Lambda_{PH}$ are in the passband and frequencies $0 \leq \lambda \leq \Lambda_{SL}$ and $\Lambda_{SH} \leq \lambda \leq \pi$ are in the

---

[1] Abraham Peled and Bede Liu, Digital Signal Processing, New York: John Wiley and Sons, 1976.

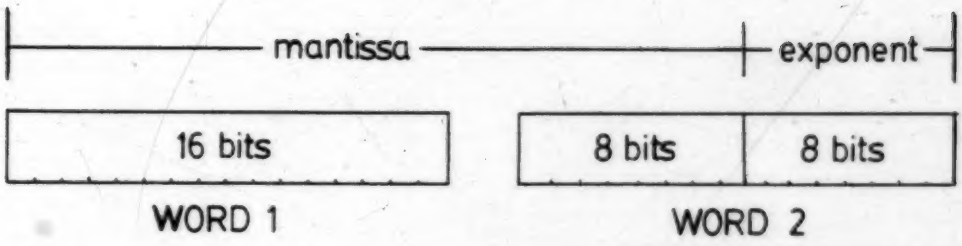

Figure 9. Single Precision Integer Format

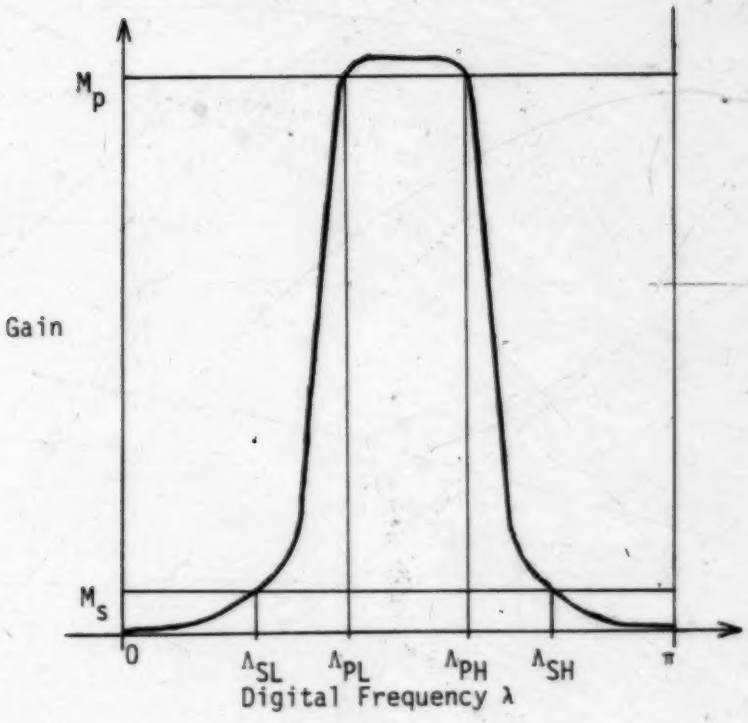

Figure 10. Bandpass Filter - General Amplitude Response

stopbands. The remaining frequencies constitute transition bands. The bilinear transformation between analog frequency, ω, and digital frequency, λ, which is applied to an analog lowpass filter to obtain a digital bandpass filter is given in equation 28.

$$\omega = \alpha(\beta - \cos\lambda)/\sin\lambda \tag{28}$$

where $\alpha = \cot[(\lambda_{PH} - \lambda_{PL})/2]$

$\beta = [\sin(\lambda_{PH} + \lambda_{PL})]/(\sin\lambda_{PH} + \sin\lambda_{PL})$

The transformation between the Laplace transform variable, s, and the z-transform variable, z, is given by equation 29.

$$s = \alpha \frac{z^2 - \beta z + 1}{z^2 - 1} \tag{29}$$

It is clear from equation 29, that for every pole in the left half of the s-plane, two poles are created inside the unit circle in the z-plane. Thus, an Nth-order analog lowpass filter will be transformed to a 2Nth-order digital bandpass filter.

Equation 29 transforms the analog frequencies -1 and +1 to digital stopband edges, λ_{PL} and λ_{PH}. Similarly, the analog frequencies

$\alpha(\beta - \cos\lambda_{SL})/\sin\lambda_{SL}$ and $\alpha(\beta - \cos\lambda_{SH})/\sin\lambda_{SH}$

map to the stopband edges, λ_{SL} and λ_{SH}, respectively.

The following frequency specifications were made for this application.

$$\Lambda_{PL} = 3\pi/16 \text{ (0.75 x pump frequency)}$$
$$\Lambda_{PH} = 5\pi/16 \text{ (1.25 x pump frequency)}$$

Note that the specifications could be made in terms of digital frequency, because the sampling rate is fixed at 8 times the pump frequency. Digital frequencies are related to analog frequencies and the sampling frequency, F_s, by $\lambda = 2\pi f/F_s$. The passband is thus centred at the pump frequency, the -3 dB points are 0.75 of the pump frequency and 1.25 of the pump frequency. The design criteria specified the need for a maximally flat filter. A Butterworth filter is the analog filter with a maximally flat amplitude response. The stopband width is determined only by the order of the Butterworth filter and so is not specified. Substituting these specified values in equations 28 and 29, the following transformation is obtained.

$$s = 5.027 \frac{(z^2 - 0.721z + 1)}{(z^2 - 1)} \qquad (30)$$

A 6-pole Butterworth low pass analog filter has an ideal stop band attenuation (M_S) of more that 30 dB and passband ripple (M_P) of less than 3 dB. The Laplace transform transfer function of such an analog filter, with the 3dB cutoff normalized to w=1 is given by the following

equation.

$$H(s)=\frac{1}{(s^2 + 0.5176s + 1)(s^2 + 1.4142s + 1)(s^2 + 1.9319s + 1)} \quad (31)$$

By using the transformation 30 in equation 31, the digital filter z-transform transfer function for the required bandpass filter is obtained.

$$H(z) = \frac{0.03957\ (z^2 - 1)^6}{D_1(z)D_2(z)D_3(z)D_4(z)D_5(z)D_6(z)} \quad (32)$$

The functions in the denominator are second degree polynomials as follows.

$$D_1(z) = z^2 - 1.1342z + 0.6636 \quad (32a)$$

$$D_2(z) = z^2 - 1.2804z + 0.6936 \quad (32b)$$

$$D_3(z) = z^2 - 1.0482z + 0.7272 \quad (32c)$$

$$D_4(z) = z^2 - 1.4422z + 0.7894 \quad (32d)$$

$$D_5(z) = z^2 - 1.0603z + 0.8882 \quad (32e)$$

$$D_6(z) = z^2 - 1.5937z + 0.9230 \quad (32f)$$

This filter was realized as a cascade connection of simpler filters corresponding to the six factors of H(z) of the form

$$H_i(z) = \frac{z^2 - 1}{z^2 + a_i z + b_i} \quad (33)$$

Thus,

$$H(z) = \prod_{i=1}^{6} H_i(z) \qquad (34)$$

where the coefficients a_i and b_i of each stage correspond to the coefficients of equations 32a to 32f. Each of the six $H_i(z)$ was individually realized in the canonical form shown in figure 11 and each becomes one of the 6 stages of the filter program. The input signal $\{x_n\}$ was inputted into stage 1 (transfer function $H_1(z)$) and the output of stage 1 became the input of stage 2. Similarly, the input of each succeeding stage was the output of the preceding stage. Output of stage 6 was the output of the filter.

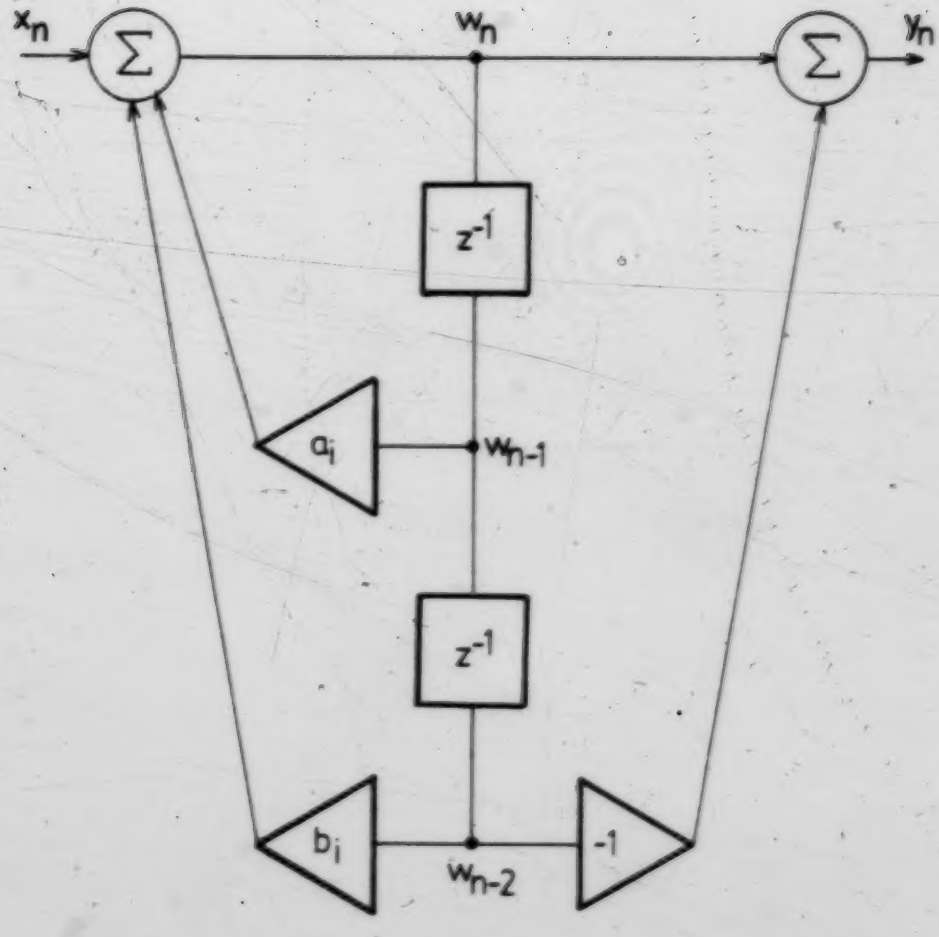

Figure 11. Second Order Digital Filter - Canonical Form

CHAPTER VI

ANALOG ANTI-ALIASING FILTER DESIGN

In designing the digital filter, an analog frequency spectrum is mapped to a desired digital frequency spectrum using the relationship given in equation 28. It should be noted that this mapping is not one-to-one, but one-to-many. A single analog frequency, ω_k, maps to an infinite number of digital frequencies given by $\lambda_n = \lambda_k + 2n\pi$ where n is any integer and λ_k is the solution to equation 28 in the range $-\pi \leq \lambda \leq \pi$. Thus, although we have mapped to a passband centred at a digital frequency of $\pi/4$, passbands are also created centred at $-\pi/4 + 2n\pi$ and $+\pi/4 + 2n\pi$ where $n>0$. To ensure that there will be no signal in any of these passbands, an anti-aliasing filter is applied to the analog input signal to attenuate any frequencies greater than one half of the sampling frequency. A filter was designed which was maximally flat in the region 0 to 4 Hz. In this region, the digital filter would select the pump frequency. Outside this region, a rapid cutoff was needed because of an aliased passband at approximately 7 Hz. An 8-pole Butterworth low pass filter was selected to achieve a roll-off of 24 dB per octave.

It was decided to utilize an active filter for this

purpose because of their small size for low frequency applications. The filter consists of four cascaded two-pole filters of the type shown in figure 12.

The voltage transfer function of this circuit is of the general form of the complex conjugate pole pair transfer function given is equation 35.

$$H(s) = \frac{H_o \omega_o^2}{s^2 + \alpha \omega_o s + \omega_o^2} \tag{35}$$

In our case,

$$H_o = - R_2/R_1 \tag{36}$$

$$\omega_o = \frac{1}{C_1 C_2 R_2 R_3}^{1/2} \tag{37}$$

and

$$\alpha = \sqrt{\frac{C_2}{C_1}} \left(\sqrt{\frac{R_3}{R_2}} + \sqrt{\frac{R_2}{R_3}} + \sqrt{\frac{R_2 R_3}{R_1}} \right) \tag{38}$$

By choosing convenient and available values for the capacitors, and defining unity DC gain and 3 dB cutoff frequency f_o = 4 Hz (ω_o = 25.13 radians/second), a suitable filter was designed using equations the following equations.

$$R_2 = \frac{\alpha}{2\omega_o C_2} \left(1 + \sqrt{1 - \frac{4C_2/C_1(1 - H_o)}{\alpha^2}} \right) \tag{39}$$

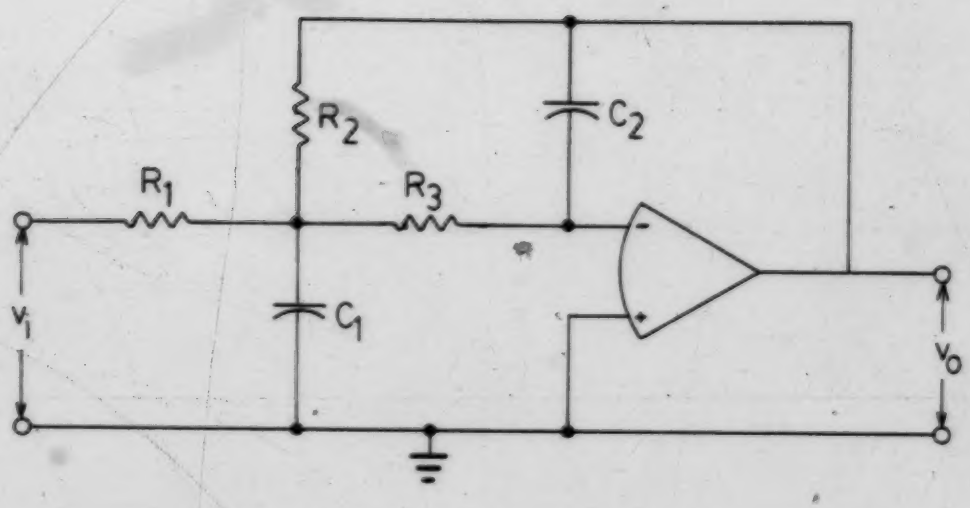

Figure 12. Two-Pole Analog Filter Schematic

$$R_1 = -R_2/H_o \tag{40}$$

$$R_3 = 1/\omega_o^2 C_1 C_2 R_2 \tag{41}$$

From tables[1], the α values required for an 8-pole Butterworth low-pass filter were found. Component selections are shown in table 2 for each of the four stages.

The capacitors were polystyrene and were measured on a Hewlett Packard 4260A universal bridge. Values in round brackets are the actual metal film resistor values used in the filter, as measured on a Simpson C464 digital multimeter. The active components of the 4 stage filter were contained on an Exar XR-084 Quad BIFET operational amplifier integrated circuit. The filter circuit itself was constructed on the microprocessor wirewrap prototype board, with input at connector P3 pin 39 and output at connector P3 pin 5.

---

[1]J.D. Graeme, G.E. Tobey, and L.P. Huetsman, (eds.), Operational Amplifiers: Design and Applications, New York: McGraw Hill Book Company, 1971.

TABLE 2

ANALOG FILTER COMPONENTS

Stage	α	[rad/sec] ω_o	H_o	[μF] C_1	[μF] C_2	[kΩ] R_1	[kΩ] R_2	[kΩ] R_3
1	1.961571	25.13	-1	1.043	0.4505	58.96 (58.9)	58.96 (58.9)	57.14 (57.1)
2	1.662939	25.13	-1	1.021	0.1012	50.82 (50.8)	50.82 (50.7)	301.5 (301)
3	1.111140	25.13	-1	1.000	0.1002	89.90 (89.9)	89.90 (89.9)	175.7 (175.6)
4	0.370181	25.13	-1	0.9925	0.00994	243.4 (244)	243.4 (244)	659.2 (660)

CHAPTER VII

RESULTS

Frequency Spectrum

After the digital filter was designed and programmed, and the analog anti-aliasing filter circuitry built, a frequency spectrum of the combined digital/analog filter system was obtained. This was obtained by connecting the output from a low frequency 3-phase oscillator, General Radio Company model T1305A, to the input of the analog anti-aliasing filter. The output of the analog filter was sampled at 8 times the pump frequency as generated by the slotted wheel and external trigger pulse circuitry. The RMS amplitude of the output of the digital filter was calculated by summing the squares of the latest 48 outputs, dividing by 48, and taking the square root. This result was displayed on the LCD display in real time, but it took approximately 2 minutes for the output to reach a steady value. The calculation of RMS output was halted after 640 samples, with the most recent value being recorded as the filter output. Filter outputs were recorded at 189 points in the range 0.01 Hertz to 100.0 Hertz. The frequency spectrum is plotted in figure 13.

FIGURE 13

SYSTEM FREQUENCY RESPONSE

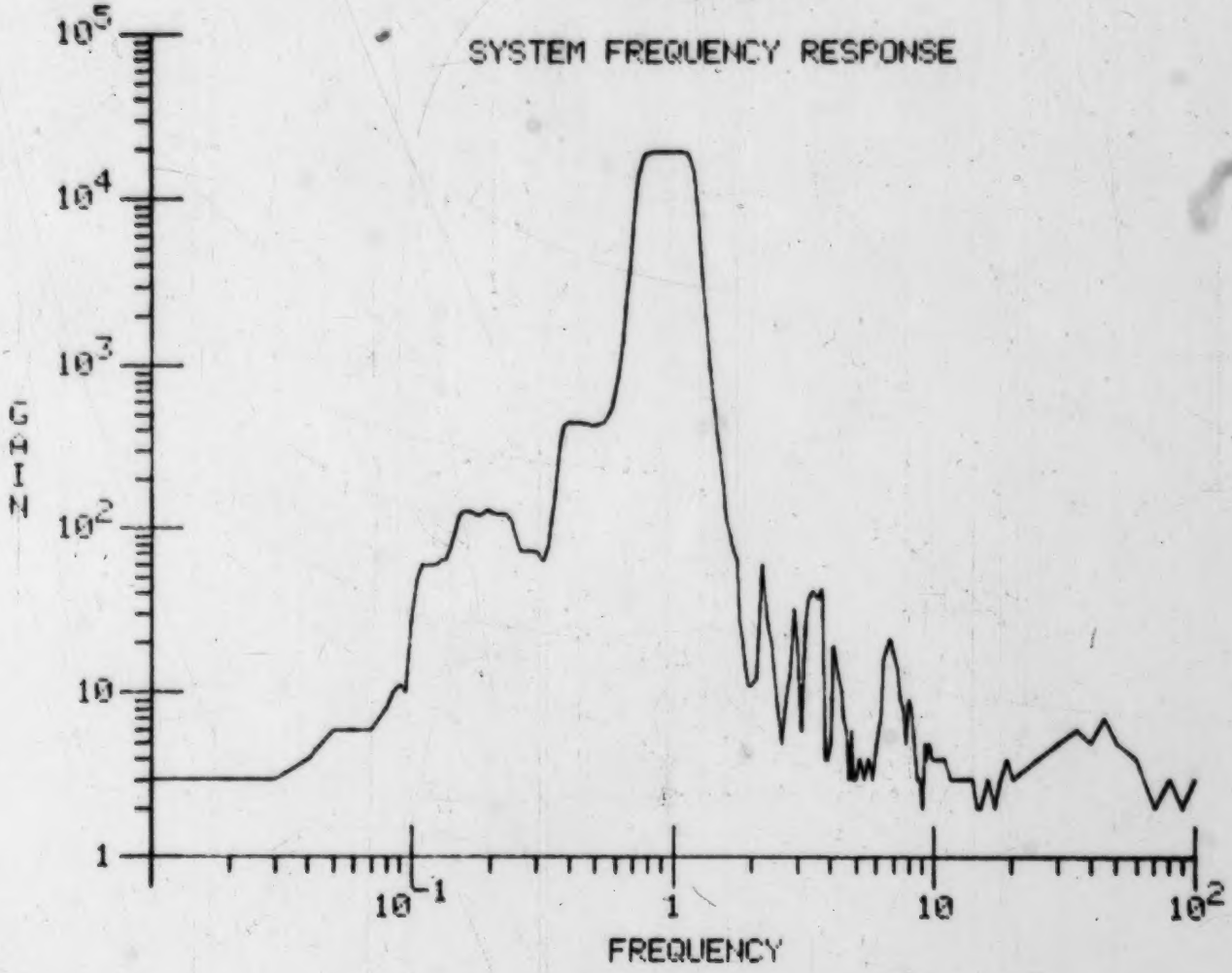

Calibration Data

Calibration data was required to define the relationship between the filter output amplitude and the incompressible volume within the box. The first set of calibration data obtained was collected over a period of three days and was performed at room temperature. The procedure was to observe the digital outputs for a bottle of known volume and containing various measured amounts of water. The digital RMS calculation and recording was identical to the procedure described for obtaining the frequency spectrum. In an effort to maintain a consistent rate of air leaking to atmosphere around the lid and gasket, care was taken to tighten the lid clamps by the same amount and in the same order, since the tensions on the clamps interact with each other. At least three outputs were recorded at 163 known volume intervals in the range of 682 millilitres to 5082 millilitres. These 163 outputs are plotted in figure 14 along with a curve representing the least squares approximation of the data to a polynomial of degree two. It should be noted that the units for the digital filter output are "uncalibrated millivolts". The digital filter gain was set at a value that would make the filter output for the largest unknown volume reach approximately 80% of the maximum number that can be displayed on the 4-digit hexadecimal LCD display. Although the digital filter output is in some sense "voltage", it has not been calibrated to any voltage

FIGURE 14

CALIBRATION CURVE - ROOM TEMPERATURE

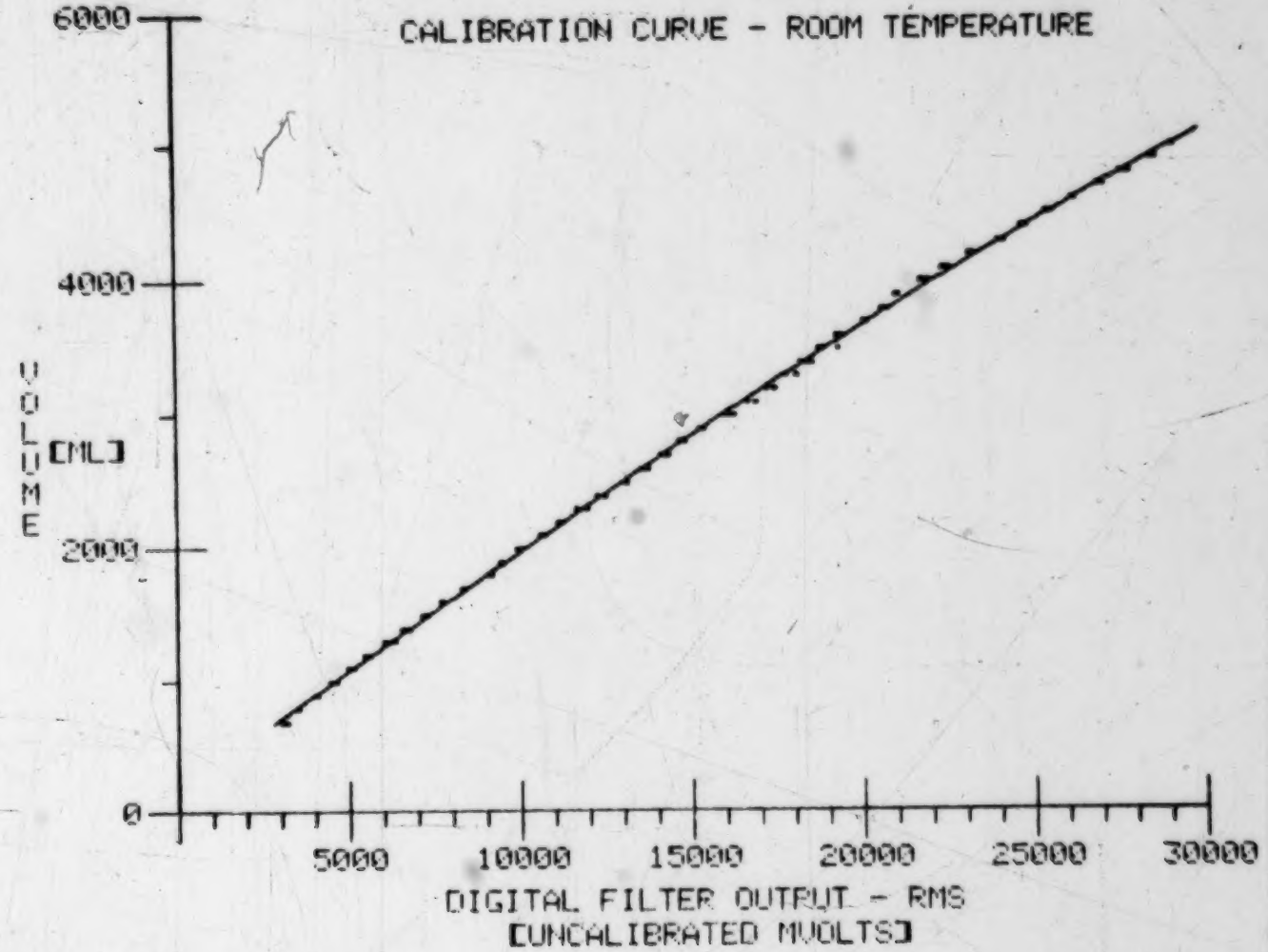

standard.

If the general form of a quadratic polynomial is

$$P(V) = a_2V^2 + a_1V^1 + a_0$$

then the coefficients a_i for the quadratic approximation to this data (expressed in litres) are

$$a_0 = -1130.$$

$$a_1 = 5980.$$

$$a_2 = 247.$$

Typical variation in the output readings at any given volume were +/- 3 percent.

The second set of calibration data was obtained with the air temperature in the box at 30 degrees Celsius and with a vinyl baby pad lining the bottom of the box. The procedure was shortened by only measuring one output at 100 millilitres volume intervals from 382 millilitres to 5047 millilitres. The calibration curve representing the least squares approximation of this data to a quadratic polynomial is plotted in figure 15.

The coefficients a_i were as follows:

$$a_0 = -24.8$$

$$a_1 = 3910.$$

$$a_2 = 344.$$

FIGURE 15

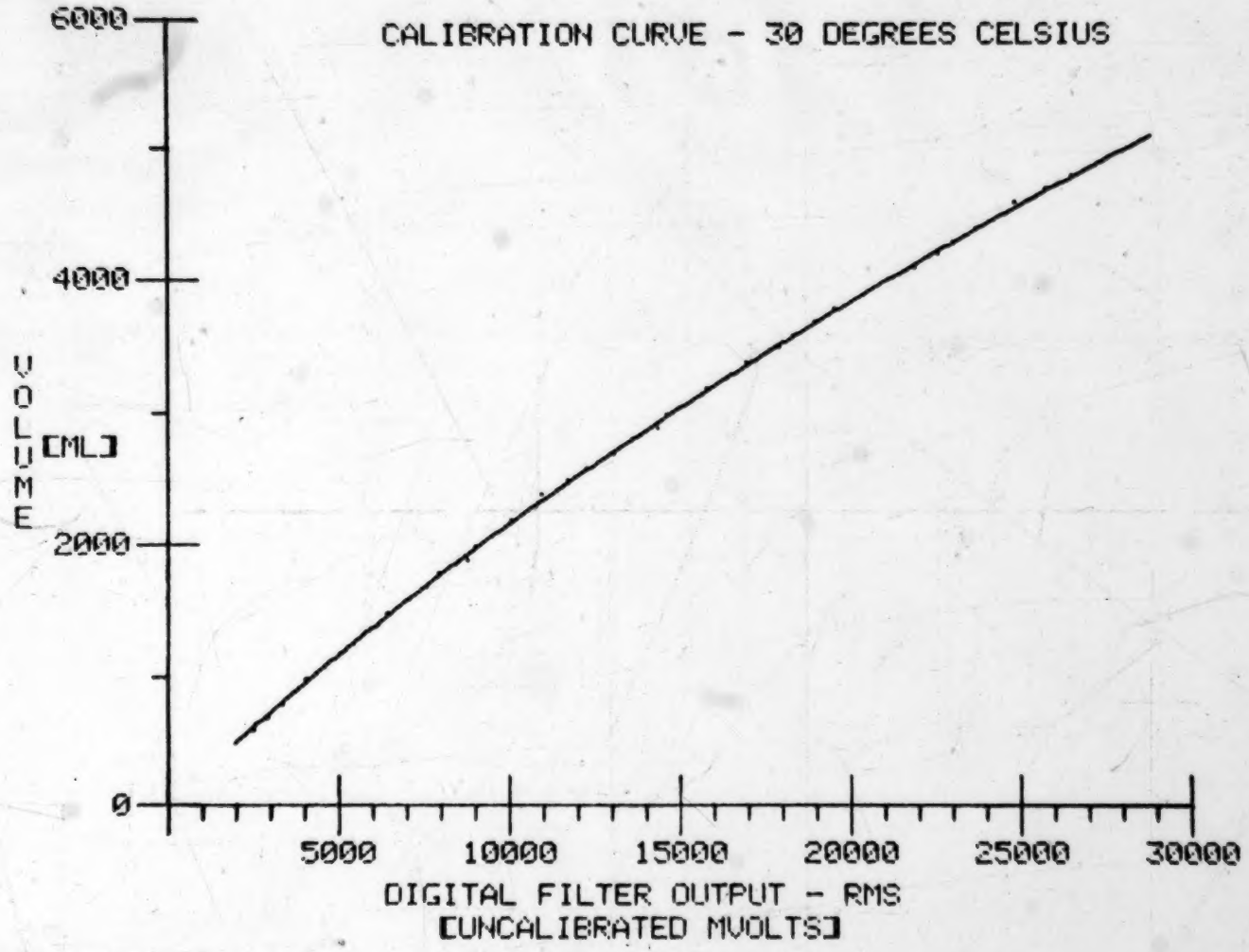
CALIBRATION CURVE - 30 DEGREES CELSIUS
6000
4000
2000
0
VOLUME [ML]
5000
10000
15000
20000
25000
30000
DIGITAL FILTER OUTPUT - RMS
[UNCALIBRATED MVOLTS]

Measurements of Unknown Volumes

These coefficients were used by an "approximation" subroutine added to the microprocessor program. This subroutine obtains a volume in millilitres from the actual digital filter output by making estimates of the volume. The algorithm for producing these estimates is described below. An initial volume estimate is made equal to one half of the maximum allowable volume. The digital filter output for this volume is calculated using the quadratic polynomial approximation formula. By comparing this "estimated" output with the actual output, the estimate is revised by adding or subtracting a correction factor. This correction factor is initially set to one quarter of the maximum volume range and is halved with each successive estimation. The digital filter output for this new volume estimate is again calculated and the process repeats itself until the difference between one estimate and the next is less than 1 millilitre. At this point, the volume estimate is printed on the CRT display.

Two types of unknown volume measurements were performed. A bottle filled with various amounts of water was measured with the air displacement equipment. The volume of water was then measured with a graduated cylinder and added to the known volume of the bottle. The two measurements were compared at 27 different points. This data is shown in table 3.

TABLE 3

UNKNOWN LIQUID VOLUME MEASUREMENTS

Volume by Graduated Cylinder	Volume by Air Displacement	Percentage Difference
380	361	-5.0
480	502	+4.6
580	594	+2.4
680	687	+1.0
780	760	-2.6
980	984	+0.41
1180	1215	+3.0
1380	1378	-0.14
1580	1551	-1.8
1780	1762	-1.0
1980	1996	+0.81
2180	2192	+0.55
2380	2399	+0.80
2580	2574	-0.23
2780	2800	+0.72
2980	2933	-1.6
3180	3168	-0.38
3380	3378	-0.059
3580	3579	-0.028
3780	3784	+0.11
3980	3993	+0.33
4180	4193	+0.31
4380	4374	-0.14
4580	4576	-0.087
4780	4776	-0.084
4980	4991	+0.22
5125	5090	-0.68

The second type of unknown volume measurement was performed using a six-month old kitten. The volume of the kitten was measured using the air displacement apparatus with the kitten in positions of sitting or lying down. Although, the volume of the kitten could not be verified using another method of volume measurement, the consistency of readings with a warm, breathing, moving animal could be assessed. This data is shown in table 4.

TABLE 4

CAT VOLUME MEASUREMENTS BY AIR DISPLACEMENT

Weight of Cat = 2575 grams

	Sitting Volume [millilitres]	Lying Volume [millilitres]
Day 1	2122	
	2158	
	2104	
		2290
Day 4	2102	
		2292
Day 7	2006	
	2006	
		2365
Day 11	2024	
	2100	
		2412
		2432
		2356
Total Runs	8	6
Mean Volume	2075	2358
Maximum Deviation from Mean	+4.0%	+3.1%
% Body Fat	Not defined	3.3

CHAPTER VIII

DISCUSSION

The equipment described in the preliminary chapters of this thesis was designed and constructed to provide a simple, accurate clinical instrument for the measurement of body fat in infants by determining body volume. As was seen in the results, a reproducible estimate of volume can be obtained for both inanimate and living objects. However, the resolution of the volume measurement using the present equipment is not sufficient for clinical or research application to measurement of body fat.

The following sections will be a discussion of the system design process, observations, results, and recommendations concerning the apparatus and testing procedure. This is done with a view to improving any future instrumentation of this sort.

Box and Pump Characteristics

Using a pressurized air system for any sort of physiological measurement requires safeguards to prevent damage to tissue from overpressure. When the whole body is exposed to a pressurized atmosphere, the organ most sensitive to overpressure is the ear. Fortunately, the

pressure of the middle ear can be equalized to that of the atmosphere through the Eustachian tubes, enabling the body to comfortably withstand much greater pressure extremes.

Unfortunately, the Eustachian tubes are not usually open and must be opened under conscious muscular control. As a result, one can assume that the pressure in the middle ear of an infant will not equalize to atmospheric pressure, especially if the atmospheric pressure is changing at frequencies greater than 0.1 Hz. The amplitude of any pressure oscillations in an infant's environment must, therefore, be kept very small. As mentioned previously, however, the differential pressure signal to be detected is an order of magnitude smaller than these absolute pressure excursions. A nulled system, in which only an object which has an incompressible volume contributes to signal amplitude, is the reason acceptable accuracy is theoretically possible.

It turns out that, in practice, a perfectly nulled system of this sort is extremely difficult to obtain. The instrument is said to be balanced when both boxes are empty, the pump is running and the absolute pressure in each box is exactly the same for all points in the pump cycle. When the differential pressure is not zero throughout the pump cycle, the boxes are said to be "out-of-balance".

A number of factors can contribute to an "out-of-balance" signal. The objectives of the first few

experiments performed with the system were to identify these factors, to determine the magnitude of their contribution to an "out-of-balance" signal, and to thereby minimize their contribution.

The two basic adjustments necessary for balancing the signal are obvious from theory:

a) sinusoidal amplitude must be the same in each box.

b) the phase angle between the sinusoids in each box must be zero.

As the following will show, these two adjustments can be treated as independent corrections to the "out-of-balance" signal.

Sinusoidal Amplitude. Once again, to distinguish the two boxes in the following analysis, we will use the X-box and E-box designations described in chapter III.

Equation 14 describes the absolute pressure within one empty box. It is rewritten below as equation 42 with $P_{\Delta E}(t)$, V_{BE} and $V_{\Delta E}$ representing the absolute pressure, box and stroke volumes in E-box, respectively.

$$P_{ATM}V_{BE} = P_{\Delta E}(t)(V_{BE} - V_{\Delta E}\sin\omega t) \qquad (42)$$

We now assume X-box is empty but has box and stroke volumes which are different from those of E-box.

$$P_{ATM}V_{BX} = P_{\Delta X}(t)(V_{BX} - V_{\Delta X}\sin\omega t) \qquad (43)$$

The differential pressure signal in this case is given by

$$P_m(t) = P_{\Delta X}(t) - P_{\Delta E}(t)$$

$$= P_{ATM}\left(\frac{1}{1 - \frac{V_{\Delta X}}{V_{BX}}\sin\omega t} - \frac{1}{1 - \frac{V_{\Delta E}}{V_{BE}}\sin\omega t}\right)$$

$$= \frac{P_{ATM}\left(\frac{V_{\Delta X}}{V_{BX}} - \frac{V_{\Delta E}}{V_{BE}}\right)\sin\omega t}{\left(1 - \frac{V_{\Delta X}}{V_{BX}}\sin\omega t\right)\left(1 - \frac{V_{\Delta E}}{V_{BE}}\sin\omega t\right)} \qquad (44)$$

This equation can be approximated because $V_{BX} >> V_{\Delta X}$ and $V_{BE} >> V_{\Delta E}$. Hence,

$$P_m(t) = P_{ATM}\left(\frac{V_{\Delta X}}{V_{BX}} - \frac{V_{\Delta E}}{V_{BE}}\right)\sin\omega t \qquad (45)$$

Thus, we obtain a sinusoid in phase with the piston cycle. A zero amplitude, or balanced, signal is possible as long as

$$\frac{V_{\Delta X}}{V_{BX}} = \frac{V_{\Delta E}}{V_{BE}} \qquad (46)$$

The fact that only the ratio of stroke volume to box volume needs to be equal in each box means that E-box can be as small or as large as the designer likes. Because the pump used in the present apparatus has a coarse stroke volume adjustment, a very fine adjustment in box volume

would be needed if a small E-box were to be balanced to the X-box ratio. In the analyses which follow, an E-box with a volume approximately equal to the X-box volume is retained.

The E-box does contain a screw-adjustable piston and this adjustment is used to balance the sinusoidal amplitude, after the stroke volumes have been equalized as much as their coarse adjustment permits.

Sinusoidal Phase. Even when the sinusoidal amplitudes had been balanced as closely as possible using the screw-adjustable piston, a phase angle error was still apparent. This can be accounted for by a phase difference between the two boxes.

If the piston in X-box leads that of E-box by a phase angle, θ, the absolute pressure in X-box is described by

$$P_{ATM}V_{BX} = P_{\Delta X}(t)(V_{BX} - V_{\Delta X}\sin(\omega t + \theta)) \qquad (47)$$

The differential pressure signal in this case is given by

$$\begin{aligned} P_m(t) &= P_{\Delta X}(t) - P_{\Delta E}(t) \\ &= P_{ATM}\left(\frac{1}{1 - \frac{V_{\Delta X}}{V_{BX}}\sin(\omega t + \theta)} - \frac{1}{1 - \frac{V_{\Delta E}}{V_{BE}}\sin\omega t}\right) \\ &= P_{ATM}\frac{\frac{V_{\Delta X}}{V_{BX}}\sin(\omega t + \theta) - \frac{V_{\Delta E}}{V_{BE}}\sin\omega t}{\left(1 - \frac{V_{\Delta X}}{V_{BX}}\sin(\omega t + \theta)\right)\left(1 - \frac{V_{\Delta E}}{V_{BE}}\sin\omega t\right)} \end{aligned} \qquad (48)$$

Making the same approximation as before, because $V_{BX} >> V_{\Delta X}$ and $V_{BE} >> V_{\Delta E}$, the denominator term becomes 1. Using the trigonometric identity,

$$\sin(A+B) = \sin(A)\cos(B) + \cos(A)\sin(B) \tag{49}$$

equation 48 reduces to

$$P_m(t) = \frac{V_{\Delta X}}{V_{BX}} (\sin(\omega t)\cos\theta + \cos(\omega t)\sin\theta) - \frac{V_{\Delta E}}{V_{BE}}\sin\omega t \tag{50}$$

But we can assume that the phase angle difference is small so that $\cos\theta \cong 1$ and $\sin\theta \cong \theta$.

$$P_m(t) \cong P_{ATM}\left[\left(\frac{V_{\Delta X}}{V_{BX}} - \frac{V_{\Delta E}}{V_{BE}}\right)\sin\omega t + \frac{V_{\Delta X}}{V_{BX}}\theta\cos\omega t\right] \tag{51}$$

However, the sinusoidal amplitudes have been approximately balanced so that

$$\frac{V_{\Delta X}}{V_{BX}} = \frac{V_{\Delta E}}{V_{BE}}$$

and

$$\cos t = \sin(\omega t + \pi/2)$$

Thus,

$$P_m(t) \cong P_{ATM} \frac{V_{\Delta X}}{V_{BX}} \theta \sin(\omega t + \pi/2) \qquad (52)$$

The evidence of a phase error is a sinusoid which leads the pump cycle by 90 degrees in phase. The amplitude of this sinusoid is proportional to the phase angle that the X-box piston leads the E-box piston.

For this reason, the balancing procedure was more difficult than just using the screw-adjustable piston to balance the stroke volume to box ratios. Near the balance point, phase lag or lead of the pressure signal with respect to the pump cycle was observed. By repositioning the angle of the X-box arm, the phase difference was reduced to zero. Although the $\cos(\omega t)$ term in equation 52 is the predominant component of an "out-of-balance" signal due to phase differences, a $\sin(\omega t)$ term, thought to have been reduced to 0 by amplitude adjustments, may reappear after phase adjustments. This is the effect of the $\sin(\omega t)\cos(\theta)$ term in equation 51. By repeating an amplitude adjustment, and alternating phase and amplitude adjustments thereafter, a point very close to the balance point was eventually achieved.

The voltage output of the transducer demodulator was connected to an oscilloscope to obtain a visual display of the differential pressure signal. The pump frequency was

low enough that the crank position could be visually compared to the oscilloscope trace, and the relative phases were judged quite easily. The iterative procedure described above was then used to balance the differential pressure signal. However, near the balance point, the unexpected presence of a second harmonic of the pump frequency in the differential pressure signal forced termination of the balancing procedure. The amplitude of the first harmonic became much less than that of the second harmonic and a quantitative assessment of the first harmonic phase relative to the pump cycle was impossible. This was the practical limit to which the system could be balanced. Further balancing would be possible only if real and imaginary Fourier coefficients of the first harmonic were available (eg. by real time fast Fourier transform (FFT)) or if the second harmonic were filtered out.

Of course, the theoretical considerations discussed to this point would indicate that reduction of second and all higher harmonic amplitudes to zero should occur at the balance point as well. There are two possible explanations for the presence of a large second harmonic component at balance.

Leaks. If a small leak in one box due to a hole in one side were present, air would be expected to flow out through the hole while the internal pressure is greater than atmospheric pressure, and air will flow in through the

hole while the internal pressure is less than atmospheric pressure. If the hole is small, the effect would be slight, but the pressure excursions would not be expected to be as large as if the box were perfectly sealed. In addition, a slight phase lead would be created because of the net increase or decrease in internal air volume during a negative or positive pressure half-cycle respectively. The absolute pressure in the box would reach zero before the piston reached the midpoint of its stroke, giving rise to the phase lead. This kind of leak would not be a serious problem since, as has been seen, sinusoidal amplitude and phase errors, from whatever the source, can be balanced out by adjusting the (stroke volume)/(box volume) ratio or the relative crank arm angle.

Leaks whose resistance to air flow change during each pump stroke can exist, as illustrated in the following two examples. As X-box is pressurized, its lid may rise against the clamps and hinge, thereby enlarging or creating leaks across the gasket. During the vacuum phase of the cycle, the lid is held tightly against its gasket and the leaks are decreased or closed. The second example of a variable leak would arise from poor piston construction. If the piston cylinder tapered slightly towards one end, leaks around the piston head would increase as the head approached the wider end and would decrease as the head approached the tapered end.

Variable leaks such as the ones mentioned affect the

pressure signal unevenly. For instance, if the leak is larger during the pressure phase of the pump cycle, the amplitude and phase of this part of the output signal will be affected. During the vacuum phase, however, when the leak is smaller or closed, there is less effect on this part of the output signal. Since only half of the pump cycle is affected, a second harmonic of the pump frequency will exist in the output signal even close to or at balance.

Box Expansion. Although the pressure within the boxes are limited to within 1% of atmospheric pressure, that pressure, applied over the large surface areas of the boxes, constitutes enough force to bow the walls of the box, depending on the rigidity of its construction. Obviously, while the walls are bowed out during the pressure phase of the cycle, the internal volume of the box is greater, and the internal pressure lower, than if the box were more rigid. Likewise, during the vacuum phase of the pump cycle, the internal volume is less, and the internal pressure greater, with a flexible box than a rigid one.

The second harmonic would arise if the box walls would not deflect in the same amount as they deflect out. If the lid to E-box is not identical to that of X-box, the second harmonic created by X-box lid expansion would not be cancelled by similar expansion in the E-box lid, and so

this harmonic will appear in the differential pressure signal.

Sampling Wheel and External Trigger Circuitry

While operating the pump, it was observed that the motor speed varied during a single rotation. Timing a spoked wheel attached to the motor shaft showed that while the motor was most heavily loaded during peak accelerations of the piston head, it slowed to 94% to 95% of its average speed. It was also observed that as the motor was in operation for long periods of time, its average speed would gradually increase. A possible cause of this acceleration is a decrease in the viscosity of the lubricating or sealing greases as they heat up while the pump is run. Also, the electrical characteristics of components in the speed control circuitry could change as the ambient temperature increases.

In any case, it was clear that if the one spectral component at the pump frequency was to be isolated from the pressure signal, that component's absolute frequency would have to change as the pump frequency changes. Since the filtering was performed digitally, the sampling pulses had to be synchronized with and triggered by the motion of the pump itself.

Digital Filter Design

Initially, it was not known how long all the operations in the digital filtering and output would take, or, more precisely, how much time it would take to perform a high order filter. The pump frequency was approximately 1 cycle per second. A three-pole Butterworth filter was designed, based on sampling rate of 4 cycles per second, with a passband centred on 1 cycle per second and having a width of 0.5 Hz. It was found that the computation time for such a filter was only approximately 0.03 seconds.

This result permitted a re-design of the filter to permit a faster sampling rate which eases restraints in the design of the analog anti-aliasing filter. Performance of the three-pole filter was acceptable, so a 6-pole filter was designed at a sampling rate of 8 cycles per second. This still allowed a passband at 1 cycle per second with comparable attenuation characteristics.

Results

The combined frequency response of the analog and digital filters shown in figure 13 shows a flat pass band centred at a frequency just less than 1 cycle per second. This frequency corresponds to the pump frequency. There is a rapid drop off outside the pass band such that the attenuation of frequencies less than 0.65 Hz. is at least 40 dB, and frequencies above 2.0 Hz. are attenuated at

least 50 dB. The analog low pass filter 3 dB cutoff frequency is at 4 Hz. and it is obvious that frequencies in aliased pass bands greater than 4 Hz. have been attenuated. However, rolloff in the stop bands is not smooth, as expected. Some of the jagged peaks are accentuated due to the logarithmic scale, particularly at the high and low frequencies where the output has a low amplitude and is rounded to the nearest integer less than 10. Closer to the passband, where the amplitude is higher, the cause of the jaggedness is less apparent. There is some error associated with each measurement because the output fluctuates around the value plotted in figure 13. If this were an absolute systematic error, the variability would appear relatively larger at lower amplitudes when plotted on a logarithmic scale. The rapid changes in output amplitude with small changes in input frequency suggest a "digital" origin. However, the digital filter was tested on an HP 2100 computer with no apparent errors, and all arithmetic underflows and overflows are trapped so as to halt further calculations.

The calibration curve results were very similar to that predicted by theory. Theoretically, the differential pressure signal created by a oscillating-stroke two-box system is a periodic function. This was found to be the case experimentally. The exact form of this function was given in chapter 2 as equation 17.

$$P_m(t) = P_{ATM} V_\Delta V_x \frac{\sin\omega t}{V_B(V_B - V_x) - V_\Delta(2V_B - V_x)\sin\omega t + V_\Delta^2 \sin^2\omega t} \quad (17)$$

Because of the periodicity of this expression, it was expressed as a Fourier series of a pump frequency and its harmonics. Although a general expression for the amplitude of each of the terms was not found, numerical integration was performed to find the amplitudes of each of the harmonics for various unknown volumes, V_x. It turned out that the relationship between each harmonic of the differential pressure signal and V_x could be very accurately described by a quadratic polynomial. In theory, the largest amplitude of any harmonic of the pump frequency should be that of the fundamental frequency (the frequency of the oscillating stroke volume).

Actual data shown in figures 14 and 15 in the previous chapter confirmed the ability to closely approximate the amplitude of the fundamental frequency as a quadratic polynomial of unknown volume, V_x. The polynomial relationship found for the equipment at room temperature was

$$F_a(V_x) = -1130 + 5980V_x + 247V_x^2 \quad (53)$$

where $F_a(V_x)$ is the actual filter output function which is uncalibrated and V_x is expressed in litres. Because the output is uncalibrated, it was necessary to perform a

scaling procedure in order to compare this relationship to that predicted by theory.

The first step in this scaling procedure was to obtain the theoretical output pressure values at each of the 163 volumes used to obtain equation 53. These values were calculated using equation 20 in chapter 2. By comparing these 163 values, F_t, to the actual uncalibrated output values, F_a, a linear transformation between the variables was obtained by fitting a straight line using least squares. This scaling transformation is given in equation 54 below.

$$F_t = 9.47E\text{-}3 + 2.16E\text{-}5F_a \qquad (54)$$

By applying this transformation to equation 53 above, a calibrated quadratic relationship was obtained.

$$F_{ac}(V_t) = (0.193 + 10.46V_x + 0.447V_x^2)*10^{-2} \qquad (55)$$

This compares favourably with the theoretically obtained relationship taken from Table 1:

$$F_t(V_x) = (-0.00437 + 10.78V_x + 0.212V_x^2)*10^{-2} \qquad (56)$$

where $F_t(V_x)$ is the theoretical filter output. The biggest discrepancy between the two equations is the magnitude of the y-intercept. This can be explained by the inability to accurately balance the two boxes. Because a zero-amplitude

first harmonic was not obtained with both boxes empty, a large y-intercept value resulted.

The actual linear coefficient is within 3% of the theoretical coefficient, validating the highly linear dependence of theoretical model. Although the quadratic coefficient of the curve fitted to the actual data is of the same order of magnitude, it is twice as large as that predicted by theory. Because much of the variation in the relation is accounted for by the linear dependence, it is likely that the confidence interval on the value of the quadratic coefficient is much wider than for the linear term.

By differentiating the uncalibrated equation 53 above and rearranging we can see that the resolution of the volume measurement as a function of the resolution of the pressure measurement is given by

$$dF_a = 5980 + 494V_x \, dV_x \qquad (57)$$

When calculated at V_x = 0.7 litre and V_x = 4.0 litres, this expression gives

a) At V_x = 700 millilitres, dV_x = 1.58E-4 dF_a

b) At V_x = 4000 millilitres, dV_x = 1.26E-4 dF_a

The actual resolution of the amplitude of the fundamental frequency was calculated as follows. When the pump was running, a hexadecimal representation of the RMS

amplitude of the fundamental frequency was being displayed in real time on the LCD display. At full scale, the RMS value displayed on the digital readout (15 bits) would fluctuate rapidly, changing every 1/8th of a pump cycle. The least significant digits changed more or less randomly while the the most significant digits remained steady. The hexadecimal display was stable to within 2 to 4 in the 7 most significant bits. This represents a measure of the pressure to a resolution of between 512 and 1024 in uncalibrated output units. Using the expressions above, the resolution of volume at V_x = 4.0 litres using this measurement technique is 65 to 130 millilitres. This corresponds to the resolution of the volumes measured in table 4 of Chapter VII.

Unfortunately, use of the equation of Siri to determine percent body fat from volume measurements requires an accuracy of approximately 0.5% to obtain a percentage body fat accuracy of 5%. The resolution calculated corresponds to an accuracy of 1.6% to 3.2%.

The cause of this poor resolution does not lie with the pressure transducer which had an output within .5% of a least-square fitted straight line. Nor is it because of inaccuracies in the digitization process (+/-1 least significant bit of 12 bits) or digital filter arithmetic (24 bits in single precision) that the resolution was poor. For the most part, the causes of poorer than expected resolution are related to deviations of the pump

and boxes from their "design parameters", as has been discussed.

Estimations of the body volume of a cat were attempted to confirm the reliability of measuring a breathing, heat- and moisture-producing animal as a subject. The runs were carried out over a period of 11 days to test reproducibility.

The pattern of behavior of the cat was the same on each of the 4 test days. Initially, it was frightened, and stood or walked around the box while the first 1 to 3 estimations were made. Then, confirming the lack of discomfort to its eardrums, the cat gradually relaxed, lay down, and fell asleep during the remaining runs.

Although the results could not be confirmed by another measurement technique, the each volume estimation of the cat while it was standing was within 4% of the mean of the observations. Similarly, while the cat was lying in the box, the estimations were within 3.1% of the mean of these observations. The most surprising aspect of these results was that the two means were 280 millilitres apart, with the volume of the cat seeming to be greater when lying down than when standing.

The reasons for this phenomenon are not clear. The cat's tissues should be incompressible so that position should not affect the volume. One explanation could be that the cat's breathing pattern changed when it was more relaxed and lying down, and the slower rate of breathing

was approximately the same as the pump frequency. High resistance in the airways then prevented the full pressurization of air in the lungs and contributed to a signal at the pump frequency.

Taylor et al.[1] have recently investigated the effects of surface area on air compression in these systems. They have postulated that materials with large surface area make the system more isothermal by providing more surface for heat exchanges. This reduces the pressure swings and makes the materials appear smaller than they should be. The data presented in this thesis confirm this observation. When the cat was laying down, the surface area provided by the ventral fur was removed, and the cat appears to have a greater volume than when standing or sitting.

---

[28]A. Taylor, Y. Aksoy, J.W. Scopes, G. du Mont and B.A. Taylor, "Development of an Air Displacement Method for Whole Body Volume Measurement of Infants," Journal of Biomedical Engineering, 7:9-17, January, 1985.

CHAPTER IX

CONCLUSIONS

The equipment described in chapters III to VI was designed to estimate unknown volumes in the range of 0.7 liters to 5 liters. Particular interest was paid to aspects of the design which would allow estimation of the body volume of infants.

Using the equipment to obtain volume estimates of both inanimate objects and a live cat indicate a practical maximum measurement resolution of 3%. A resolution in the volume measurement of at least .5% was required in order to use the equation of Siri to determine body fat composition.

Experience with this equipment has suggested a number of ways that the equipment design could be improved in an effort to improve the measurement resolution. Probably the most effective way to make the zero adjustment simpler is to use stepping motors to generate the oscillating stroke volume. The phase and amplitude adjustments of a modified respirator, as used in this case, are very coarse. Stepping motors would allow the digital construction of a purely sinusoidal driving force with easily adjustable stroke amplitude. Separate motors could allow for independent phase adjustment using an electrical

rather than a mechanical adjustment. One additional advantage of stepping motors with respect to servo or dc motors would be the ease of experimentation with other driving force waveforms. It could be, for instance, that a waveform could be constructed which would produce less of a second harmonic. Another example of this flexibility is that by introducing slight distortions to a sine wave, compensation could be made for asymmetrical leaks or box expansion.

A better method of sealing the box which must opened and closed must be devised. Spring-loaded clamps would create a consistent sealing pressure as long as a gasket material could be found which would seal the box under this pressure.

Because box expansion was also observed with the present equipment, heavier gauge plexiglass, or reinforcing bars along the large sides, would be required. This would prevent ~~the~~ bowing of the sides when the box is pressurized.

A better method of heating the box for the comfort of the infant should be devised. The heat lamp created too high a temperature on the plexiglass right under the lamp. Also, it took 30 minutes to warm the box to 30 degrees Celsius before beginning experimentation. An electrical heater inside the box would be satisfactory, as long as precautions were taken to prevent overheating any bedding or burning the infant.

The equipment and results described in this thesis are encouraging for a first prototype. With the refinements described above, the measurement resolution should be much closer to theory, as well as being closer to that required for body composition estimation.

BIBLIOGRAPHY

Allen, Thomas H. "Measurement of Human Body Fat: A Quantitative Method Suited for Use by Aviation Medical Officers," Aerospace Medicine, 34:907-909, October, 1963.

Analog Devices Instruments and Systems. RTI-1240/1241 User's Reference Manual, Norwood, Massachussetts: Analog Devices Inc.

Behnke, Albert R. "Absorption and Elimination of Gases of the Body in Relation to its Fat and Water Content," Medicine 24:359, 1945.

_____. "The Estimation of Lean Body Weight from 'Skeletal' Measurements," Human Biology, 31:295-315, 1959.

_____. "Quantitative Assessment of Body Build," Journal of Applied Physiology, 16:960-980, 1961.

_____. "Anthropometric Evaluation of Body Build," Annals of the New York Academy of Sciences, 110:450-464, September, 1963.

_____, Feen, B.G., and Welham W.W. "The Specific Gravity of Healthy Men," Journal of the American Medical Association, 118:495-498, 1942.

_____, and Wilmore, Jack H. Evaluation and Regulation of Body Build and Composition, New Jersey: Prentice Hall, 1974. 238 pp.

Brozek, Jozef, and Keys, A. "The Evaluation of Leanness-Fatness in Man: Norms and Interrelationships," British Journal of Nutrition, 5:194-206, 1951.

Brozek, Jozef, Grande, F., Anderson, J.T., and Keys A. "Densitometric Analysis of Body Composition: Revision of Some Quantitative Assumptions," Annals of the New York Academy of Sciences, 110:113-140, September, 1963.

Chien, S., Peng, M.T., Chen, K.P., Huang, T.F., Chang, C., and Fang, H.S. "Longitudinal Studies on Adipose Tissue and its Distribution in Human Subjects," Journal of Applied Physiology 39:825-830, 1975.

Clark, Dale A., Kay, Thomas D., Tatsch, Robert F., and Theis, Clarence F. "Estimations of Body Composition by Various Methods," Aviation, Space and Environmental Medicine, 48(8):701-704, August, 1977.

Craig, Albert B., and Ware, Donald E. "Effect of Immersion on Vital Capacity and Residual Volume of the Lungs," Journal of Applied Physiology, 23:423-425, 1967.

Cureton, Kirk J., Boileau, Richard A., and Lohman, Timothy G. "A Comparison of Densitometric, Potassium-40, and Skinfold Estimates in Prepubescent Boys," Human Biology, 47(3):321-336, September, 1975.

Durnin, J.V.G.A. , and Rahaman, M.M. "The Assessment of the Amount of Fat in the Human Body from Measurements of Skinfold Thicknesses," British Journal of Nutrition, 21:681-689, 1967.

Durnin, J.V.G.A., and Womersley, J. "Body Fat Assessed from Total Body Density and its Estimation from Skinfold Thickness: Measurements on 481 Men and Women Aged from 16 to 72 Years," British Journal of Nutrition, 32:77-97, July, 1974.

Falkner, F. "An Air-Displacement Method of Measuring Body Volume in Babies: A Preliminary Communication," Annals of the New York Academy of Sciences, 110:75-79, September, 1963.

Fomon, S.J., Jensen, R.L., and Owen, J.M. "Determination of Body Volume of Infants by a Method of Helium Displacement," Annals of the New York Academy of Sciences, 110:80-90, September, 1963.

Forbes, G.B. "Methods for Determining Body Composition of the Human Body," Pediatrics, 29:441-494, 1962.

_____, Gallup, J., and Hursh, J.B. "Estimation of Total Body Fat from Potassium-40 Content," Science, 133:101-102, 1961.

Fuchs, Robert J., Theis, Clarence F., and Lancaster, Col. Malcolm C. "A Nomogram to Predict Lean Body Mass in Men," American Journal of Clinical Nutrition, 31(4):673-678, April, 1978.

Garn, Stanley M. In: Techniques for Measuring Body Composition, Brozek, Jozef, and Henschel, Austin (eds.), p. 36, Washington: National Academy Science and Natural Research Council, 1961. 300 pp.

_____. "Human Biology and Research in Body Composition," Annals of the New York Academy of Sciences, 110:429-446, September, 1963.

Garrow, J.S., Diethelm, R., and Stallex, S.F. "An Apparatus for Measuring the Density of Obese Subjects," Journal of Physiology, 267:14P, 1977.

Girandola, Robert N., Wiswell, Robert A., Mohler, John G., Romero, Gary T., and Barnes, William S. "Effects of Water Immersion on Lung Volumes: Implications for Body Composition Analysis," Journal of Applied Physiology, 43(2):276-279, August, 1977.

Gnaedinger, R.H., Reineke, E.P., Pearson, A.M., et al. "Determination of Body Density by Air Displacement, Helium Dilution, and Underwater Weighing," Annals of the New York Academy of Sciences, 110:96-108, September, 1963.

Graeme, J.D., Tobey, G.E., and Huetsman, L.P. (eds.). Operational Amplifiers: Design and Applications, New York: McGraw Hill Book Company, 1971.

Harsha, David W., Frerichs, Ralph R., Berenson, Gerald S. "Densitometry and Anthropometry of Black and White Children," Human Biology, 50(3):261-280, September, 1978.

Hayes, John P. Computer Architecture and Organization. New York: McGraw Hill Book Company, 1978.

Heath, T.H. The Works of Archimedes. New York: Dover Publications Inc., 1953.

Jackson, Andrew S., and Pollock, Michael, L. "Prediction Accuracy of Body Density, Lean Body Weight, and Total Body Volume Equations," Medical Science in Sports, 9(4):197-201, Winter, 1977.

Jones, P.R.M., and Norgan, N.G. "A Simple System for the Determination of Human Body Density by Underwater Weighing," Journal of Physiology, 239(2):71P-73P, June, 1974.

Kagan, Benjamin M., Stanicova, Vera, Felix, Natalia S., Hodgman, Joan, and Kalman, David. "Body Composition of Premature Infants: Relation to Nutrition," American Journal of Clinical Nutrition, 25:1153-1164, November, 1972.

Katch, Frank I. "Apparent Body Density and Variability During Underwater Weighing," American Association of Health, Physical Education and Recreation Research Quarterly, 39:993-997, 1968.

_____, Michael, E.E., and Horvath, S.M. "Estimation of Body Volume by Underwater Weighing: Description of a Simple Method," Journal of Applied Physiology, 23:811-813, 1967.

_____, and Michael, E.E. "Prediction of Body Density from Skinfold and Girth Measurements of College Females," Journal of Applied Physiology, 25:92-94, 1968.

_____, and McArdle, William D. "Prediction of Body Density from Simple Anthropometric Measurements in College-Age Men and Women," Human Biology, 45:445-447, 1973.

_____, and _____. "Validity of Body Composition Prediction Equations for College Men and Women," American Journal of Clinical Nutrition, 28:105-109, 1975.

Kerlinger, Frederick N., and Pedhauser, E.S. Multiple Regression in Behaviour Research, New York: Holt, Rinehart, and Winston, 1973.

Keys, A., and Brozek, Jozef. "Body Fat in Adult Men," Physiological Reviews, 33:345-425, 1953.

Krzywicki, H.J., Ward, G.M., Rahman, D.P., et al. "A Comparison of Methods for Estimating Human Body Composition," American Journal of Clinical Nutrition, 27(12):1380-1385, December, 1974.

Lesser, Gerson T., Perl William, and Steele, Murray J. "Determination of Total Body Fat by Absorption of an Inert Gas; Measurements and Results in Normal Human Subjects," Journal of Clinical Investigation, 39:1791-1806, 1960.

Pascale, Luke R., Grossman Morton I., Sloane, Harry S., and Frankel Toby F. "Correlations Between Skinfolds and Body Density in 88 Soldiers," Human Biology, 28:165-176, 1956.

Pearse, R., Scopes, J., and Taylor, A. "The Measurement of Body Volume in Infants by Air Displacement," Proceedings: Journal of Physiology (London), 256(1):5P, March, 1976.

Peled, Abraham, and Liu, Bede. Digital Signal Processing, New York: John Wiley and Sons, 1976.

Pierson, W.R. "A Photogrammetric Technique for the Estimation of Surface Area and Volume," Annals of the New York Academy of Sciences, 110:109-112, September, 1963.

Pitts, G.E. "Studies of Gross Body Composition by Direct Dissection," Annals of the New York Academy of Sciences, 110:11-22, September, 1963.

Pollock, M.L., Loughridge, Coleman B., Linnerud, A.C., and Jackson A. "Prediction of Body Density in Young and Middle-Aged Women," Journal of Applied Physiology, 38:745-749, 1975.

Pollock, M.L., Hickman, T., Kendruck, Z., Jackson, A., Linnerud, A.C., and Dawson, G. "Prediction of Body Density in Young and Middle-Aged Men," Journal of Applied Physiology, 40:300-304, 1976.

Raja, Chand, Singh, Raghbir, Singh, H. Bharadwaj, and Singh, Indera P. "Relationship of Extremity Volumes with Total Body Volume and Body Density in Young Girls," Human Biology, 50(2):103-113, May, 1978.

Simpson, William D., Lueckee, Gerald, Cannon, Don L., and Clemens, David H. 9900 Family Systems Design and Data Book, Houston: Texas Instruments Incorporated, 1978.

Siri, W.E. In: Advances in Biological and Medical Physics. Lawrence, J.H., and Tobial, C.A. (eds.) New York: Academic Press, 1956.

Siri, W.E. In: Techniques for Measuring Body Composition. Brozek, Jozef, and Henschel Austin, (eds.) Washington: National Academy of Sciences National Research Council, 1961.

Sloan, A.W. "Estimation of Body Fat in Young Men," Journal of Applied Physiology, 23:311-315, 1967.

_____, Burt, J.J., and Blyth C.S. "Estimation of Body Fat in Young Women," Journal of Applied Physiology, 17:967-970, 1962.

Stansell, Marion J., and Hyder Jr., Anthony K. "Simplified Body Composition Analysis using Deuterium Dilution and Deuteron Disintegration," Aviation, Space, and Environmental Medicine, 47(8):839-845, August, 1976.

Taylor, A., Aksoy, Y., Scopes, J.W., du Mont, G., and Taylor, B.A. "Development of a Method for Whole Body Volume Measurement of Infants," Journal of Biomedical Engineering, 7:9-17, January, 1985.

Texas Instruments Incorporated Semiconductor Group. TMS 9900 Microprocessor Data Manual, Houston: Texas Instruments Incorporated, 1978.

Texas Instruments Incorporated Semiconductor Group. TMS 9901 Programmable Systems Interface, Houston: Texas Instruments Incorporated, 1978.

Texas Instruments Incorporated Semiconductor Group. TMS 9902 Asynchronous Communications Controller, Houston: Texas Instruments Incorporated, 1978.

Walser, M., and Stein, N. "Determination of Specific Gravity of Intact Animals by Helium Displacement; Comparison with Water Displacement," Proceedings of the Society of Experimental Biology and Medicine, 82:774-777, April, 1953.

Ward, A., Pollock, M.L., Ayres, J., Pape, G., and Jackson, A. "A Comparison of Body Density Determined by Hydrostatic Weighing and Volume Displacement," American Journal of Physiology, 234(1):E96-96, January, 1978.

Wedgwood, R.J. "Inconsistency of Lean Body Mass," Annals of the New York Academy of Science, 110:141-152, September, 1963.

Weltman, Arthur, and Katch, Victor L. "A Non-Population-Specific Method for Predicting Total Body Volume and Percent Fat," Human Biology, 50(2):151-158, May, 1978.

Willman, T.L., and Behnke, A.R. "Residual Lung Volume Determination by Methods of Helium Substitution and Volume Expansion," American Journal of Physiology, 153:138-142, April, 1948.

Wilmore, J.H. "A Simplified Method for Determination of Residual Lung Volumes," Journal of Applied Physiology, 27:96-100, July, 1969.

_____, and Behnke, A.R. "Predictability of Lean Body Weight Through Anthropometric Assessment in College Men," Journal of Applied Physiology, 25:349-355, 1968.

_____, and _____. "Anthropometric Estimation of Body Density and Lean Body Weight in Young Women," American Journal of Clinical Nutrition, 23:267-274, 1970.

Wright, H.F., and Wilmore, J.H. "Estimation of Relative Body Fat and Lean Body Weight in a United States Marine Corps Population," Aerospace Medicine, 45:301-306, 1974.

APPENDIX A

VOLUME MEASUREMENT SYSTEM
Program Flowchart
Page 1 of 5

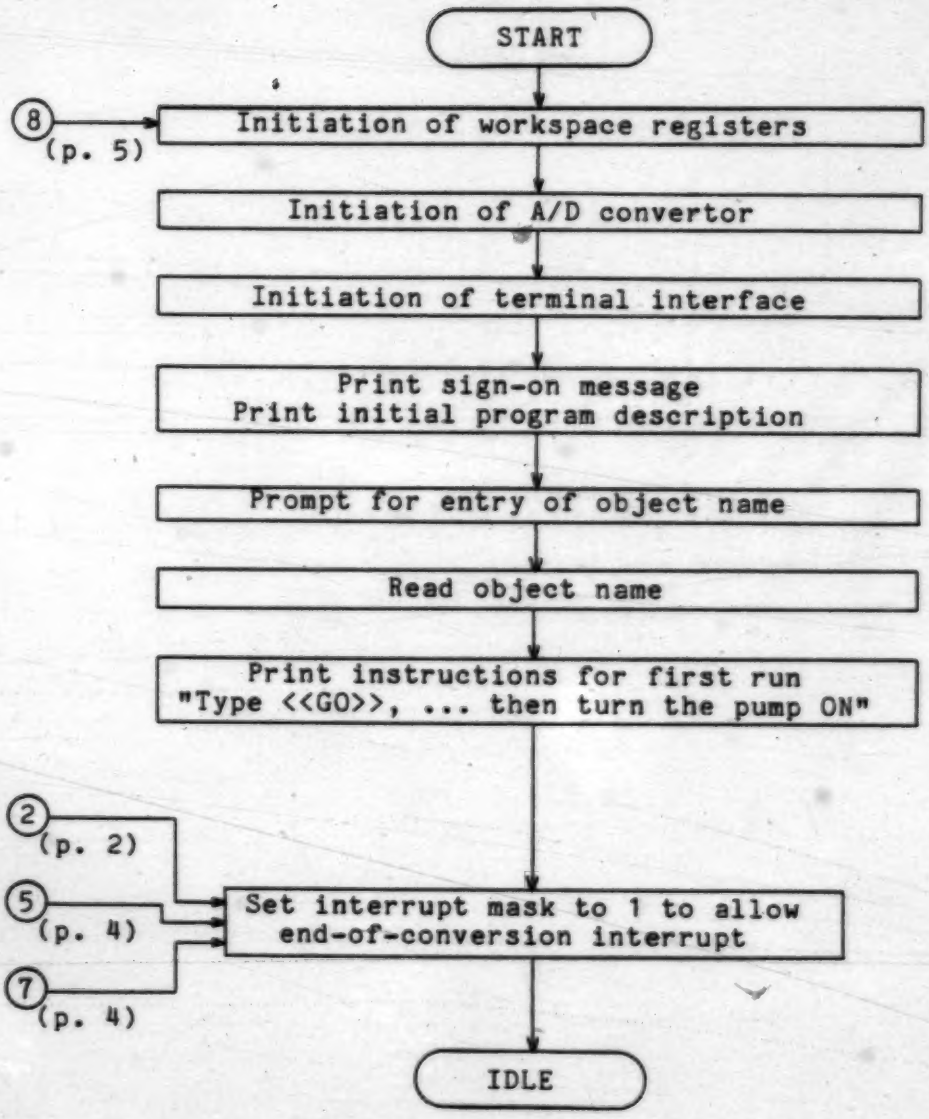

VOLUME MEASUREMENT SYSTEM
Program Flowchart
Page 2 of 5

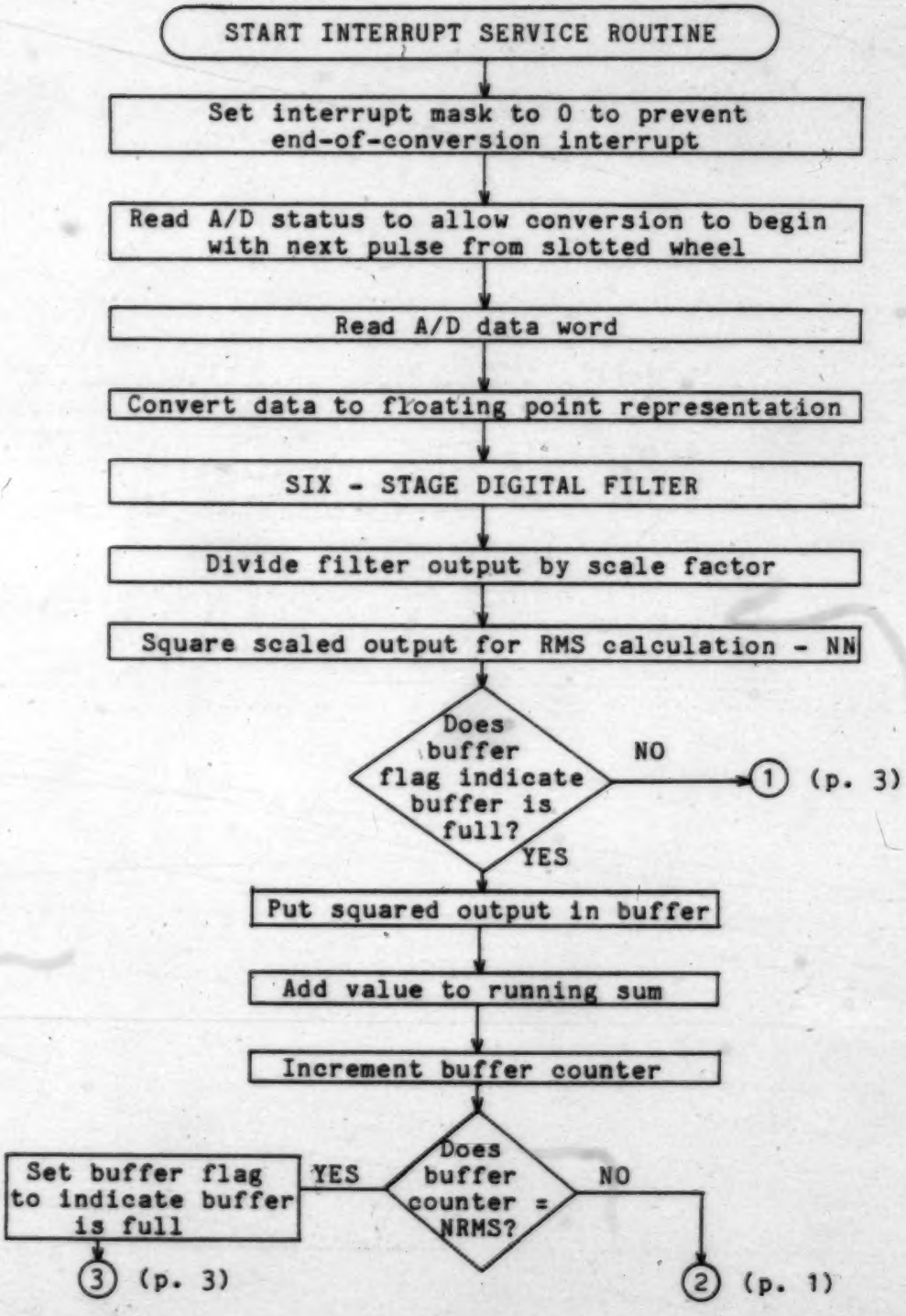
START INTERRUPT SERVICE ROUTINE
Set interrupt mask to 0 to prevent end-of-conversion interrupt
Read A/D status to allow conversion to begin with next pulse from slotted wheel
Read A/D data word
Convert data to floating point representation
SIX - STAGE DIGITAL FILTER
Divide filter output by scale factor
Square scaled output for RMS calculation - NN
Does buffer flag indicate buffer is full?
NO
1 (p. 3)
YES
Put squared output in buffer
Add value to running sum
Increment buffer counter
Does buffer counter = NRMS?
YES
Set buffer flag to indicate buffer is full
3 (p. 3)
NO
2 (p. 1)

VOLUME MEASUREMENT SYSTEM
Program Flowchart
Page 3 of 5

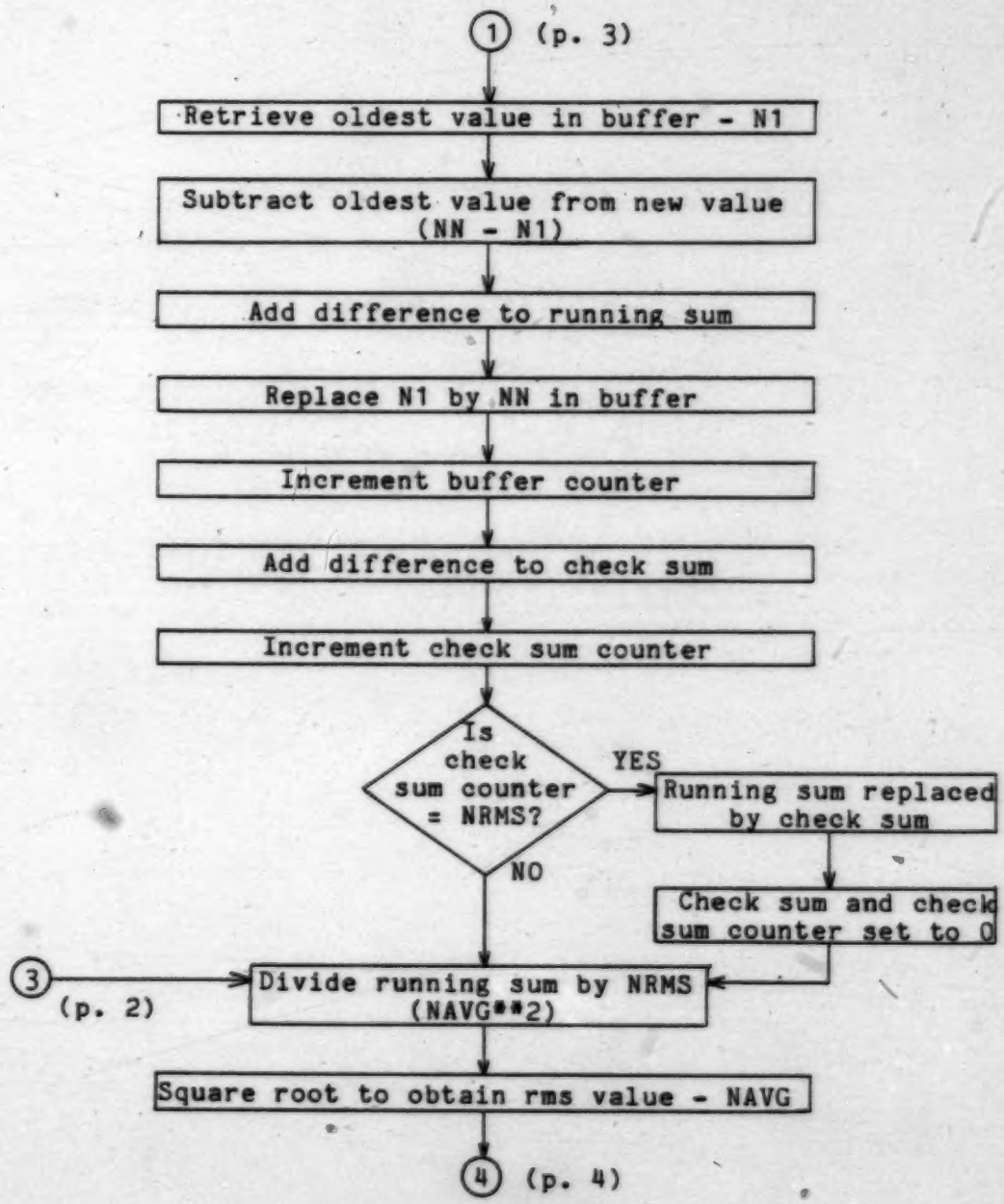
1
(p. 3)
Retrieve oldest value in buffer - N1
Subtract oldest value from new value (NN - N1)
Add difference to running sum
Replace N1 by NN in buffer
Increment buffer counter
Add difference to check sum
Increment check sum counter
Is check sum counter = NRMS?
YES
Running sum replaced by check sum
Check sum and check sum counter set to 0
NO
3
(p. 2)
Divide running sum by NRMS (NAVG**2)
Square root to obtain rms value - NAVG
4
(p. 4)

VOLUME MEASUREMENT SYSTEM
Program Flowchart
Page 4 of 5

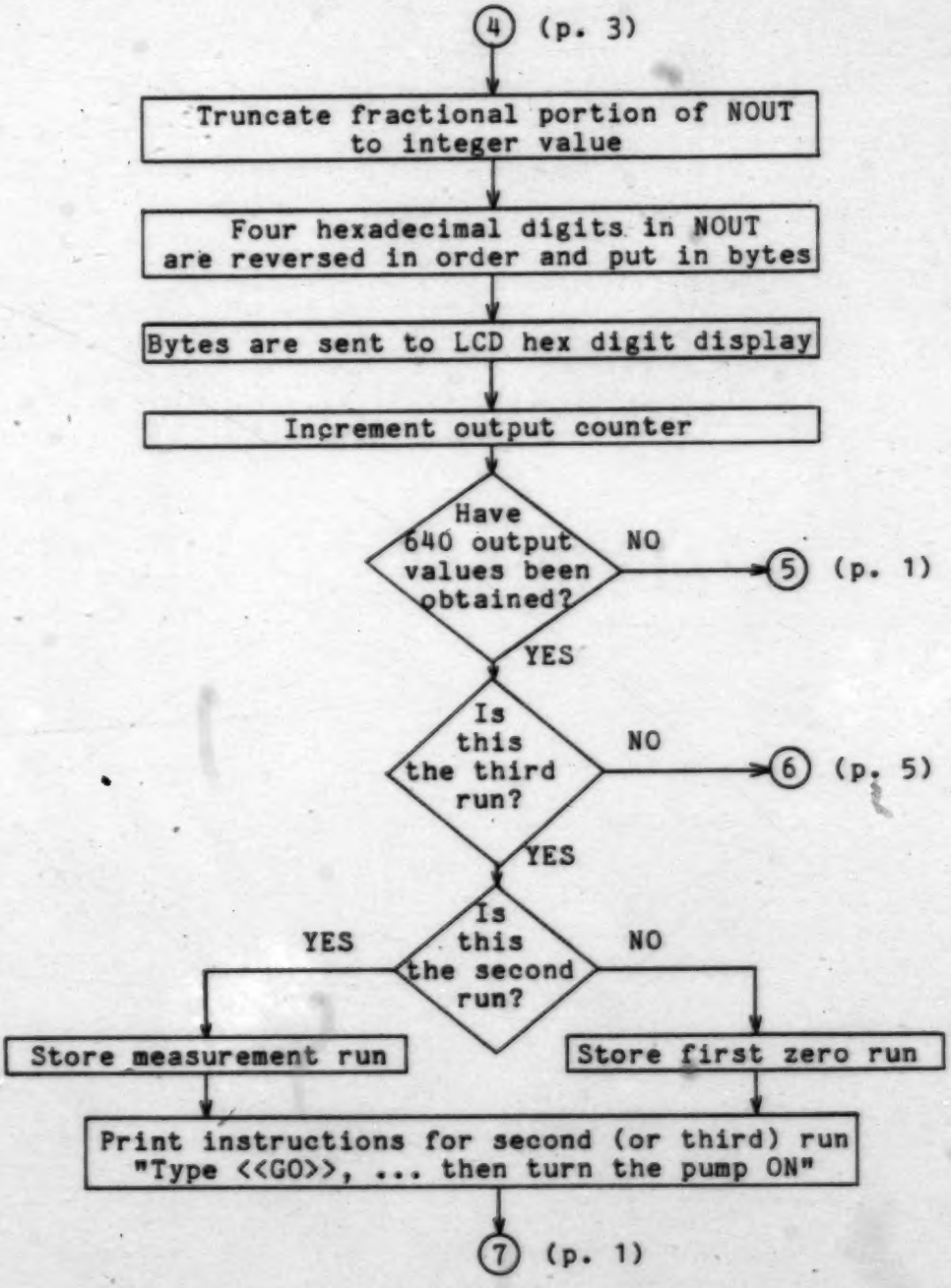
4 (p. 3)
Truncate fractional portion of NOUT to integer value
Four hexadecimal digits in NOUT are reversed in order and put in bytes
Bytes are sent to LCD hex digit display
Increment output counter
Have 640 output values been obtained?
NO
5 (p. 1)
YES
Is this the third run?
NO
6 (p. 5)
YES
Is this the second run?
YES
NO
Store measurement run
Store first zero run
Print instructions for second (or third) run "Type <<GO>>, ... then turn the pump ON"
7 (p. 1)

VOLUME MEASUREMENT SYSTEM
Program Flowchart
Page 5 of 5